NATIONAL ADVISORY COMMITTEE FOR AERONAUTICS

TECHNICAL NOTE 3509

A STUDY OF BOUNDARY-LAYER TRANSITION AND SURFACE TEMPERATURE DISTRIBUTIONS AT MACH 3.12

By Paul F. Brinich

Lewis Flight Propulsion Laboratory
Cleveland, Ohio

Washington
July 1955

NATIONAL ADVISORY COMMITTEE FOR AERONAUTICS

TECHNICAL NOTE 3509

A STUDY OF BOUNDARY-LAYER TRANSITION AND SURFACE TEMPERATURE DISTRIBUTIONS AT MACH 3.12

By Paul F. Brinich

SUMMARY

Surface temperature distributions on a hollow cylinder alined with the airstream were studied in a Mach 3.12 wind tunnel at Reynolds numbers per inch from 1×10^5 to 7×10^5. Transition with and without single roughness elements was observed from the surface temperature distributions and from high-speed schlieren motion pictures.

Comparison of the surface temperature distributions obtained on the present model with those obtained in earlier cylinder tests indicates that, as the leading edge was made sharper, the temperature rise at the transition point became more abrupt; also, the temperature distribution became more similar to that observed on a cone under the same test conditions. Sharpening the leading edge also decreased the transition Reynolds number.

When a single roughness element was located in the laminar boundary layer, the surface temperature distribution was changed only slightly at the element, but the transition point was shifted upstream somewhat. When the roughness element was placed in the transitional or turbulent boundary layer, large perturbations in the temperature distribution resulted, with no change in transition Reynolds number.

INTRODUCTION

Boundary-layer theory has advanced to the stage where it is now possible to predict with some confidence the behavior of the laminar and turbulent boundary layers on a flat plate at moderately high Mach numbers. The determination of the over-all behavior of the boundary layer, however, has lagged because of a poor understanding of the intermediate transition region, its location and extent. This report represents a continuation of the transition studies in high-speed flows with negligible pressure gradients made at the NACA Lewis laboratory and discussed in references 1 and 2.

Reference 1, which shows that the transition point fluctuates rapidly fore and aft along a body in a random manner, hypothesizes that the more or less gradual rise of the surface temperature in the transition region is related to the transition-point fluctuations. Whereas the transition studies of reference 1 were made on a cone, reference 2 extended the surface temperature measuring technique to a cylinder alined with the air flow. Comparison of the results of references 1 and 2 indicates that temperature distributions in the vicinity of transition differ markedly for the cone and the cylinder, and that the temperature distribution for the cylinder can not be directly related to the statistical distribution of the instantaneous transition-point locations. Therefore, part of the purpose of the present tests was to determine additional factors having a bearing on the surface temperature distribution in the vicinity of transition on a cylinder.

During the course of the experiments in which the effect of roughness on transition was being studied (ref. 2), certain anomalies in the temperature distributions were noted whenever the roughness element was placed in the transitional or turbulent-boundary-layer regions. A short study to confirm and explore these anomalies was accordingly made, the results of which form the second part of the present report.

Since this experiment was performed in one particular wind tunnel, it is necessary to exercise caution in applying certain of the quantitative results to other wind tunnels or to free-flight problems in which the stream turbulence differs from the present values.

APPARATUS AND TEST PROCEDURE

Cylinder Model and Instrumentation

The 5.31-inch-diameter hollow cylinder used for the present investigation is the same model as described in reference 2, except that a replaceable leading edge and static-pressure orifices have been added. A drawing giving pertinent dimensions of the model, thermocouple and static-pressure instrumentation, and the leading-edge modification is shown in figure 1. The change in the leading-edge construction was made to provide greater ease of leading-edge repair with improved machining accuracy. Since the leading edge used in the tests of reference 2 was integral with the soft outer stainless-steel shell, it was necessary to keep it at least 0.006 inch thick to meet adequate strength requirements. The present replaceable leading edge was made of hardened carbon steel, which could be machined more closely to the ideal wedge shape, and had an apex of only 0.0008-inch thickness. A slight irregularity at the juncture of the leading edge and the stainless-steel shell was formed which never exceeded 0.0005 inch. Such an irregularity could have no perceptible effect on the location of transition, according to the results of reference 2.

Single roughness elements made of 0.010-, 0.032-, and 0.079-inch-diameter wire, similar to the ones of reference 2, were used in the present investigation. The 0.032-inch element was tested at 2, 4, 8, and 12 inches from the leading edge, and the 0.010- and 0.079-inch elements at the 12-inch position only.

Surface temperatures were obtained by measuring the electrical outputs of 50 stainless-steel - constantan thermocouples. These outputs were measured on a self-balancing potentiometer having a total scale deflection of 1 millivolt, giving temperature errors less than $\pm 0.25^{\circ}$ F. Model and tunnel wall static pressures were measured on butyl phthalate differential manometers that had an accuracy of ± 0.002 pound per square inch. Schlieren high-speed motion pictures were taken with a lens system giving a 16 to 1 magnification in the direction normal to the flow, as described in reference 3. This magnification produced a virtual thickening of the boundary layer and made the laminar, transitional, and turbulent regions readily observable.

Wind Tunnel and Test Conditions

The model was tested in the NACA Lewis 1- by 1-foot variable Reynolds number tunnel at Mach 3.12, which is the same test facility used in references 1 and 2. The turbulent intensity noted previously (ref. 2) in the tunnel entrance may, therefore, be assumed to be unchanged for the present tests.

In reference 2 the model leading edge was located upstream of the schlieren field of view. Since this was an undesirable situation, the model was displaced downstream 1.8 inches to make the leading edge visible. An additional downstream longitudinal adjustment of 3.3 inches was also provided in order to study any possible effect of model location relative to the tunnel test section on the recovery-factor distribution and transition location.

The majority of the tests were conducted with the model in the forward position with the leading edge visible, and one check run was made in the displaced position 3.3 inches downstream. Temperature and pressure distributions were obtained along the bottom of the model only, as indicated in figure 1. Stagnation temperatures were maintained between 48° and 64° F, and stagnation pressures were varied from 7 to 50 pounds per square inch absolute. This gave a Reynolds number range from 1×10^5 to 7×10^5 per inch.

RESULTS AND DISCUSSION

It is generally believed that the important variables affecting transition location are Mach number, Reynolds number, pressure gradient,

heat transfer, turbulence level, leading-edge thickness, and surface roughness. Of these, only the stream Reynolds number, leading-edge thickness, and size and location of roughness elements were studied.

Pressure Distributions

The variation of the pressure coefficient C_p along the bottom of the cylinder is presented in figure 2(a) for four values of free-stream Reynolds number per inch U_∞/ν_∞. These distributions indicate a gradual increase in pressure over the entire cylinder length with small local perturbations. As was demonstrated in reference 2, pressure gradients of such magnitude would have a negligible effect on boundary-layer stability and, it may be inferred, a negligible effect on the location of transition.

Figures 2(b) to (d) show the variation of pressure coefficient for roughness elements 0.010, 0.032, and 0.079 inch high, respectively, placed 12 inches from the leading edge. With the exception of the pressure coefficient at $x = 12.4$ inches, no apparent effect of the roughness element on the pressure distribution can be noted. The remainder of the pressure distribution resembles very closely that obtained without a roughness element as shown in figure 2(a).

Figures 2(c) and (e) to (g) give the variation of pressure coefficient along the bottom of the cylinder at various values of Reynolds number per inch for a roughness element 0.032 inch high located at $x = 12$, 8, 4, and 2 inches, respectively. In these figures it is again apparent that the pressure distribution does not change markedly from that observed without a roughness element, with the exception possibly of the pressure coefficient immediately downstream of the element. In general, the coefficient at this location (0.4 in. from the element) drops below the value obtained without an element, this drop being largest for elements nearest the leading edge. At the next nearest orifices 1.6 inch upstream and 2.4 inches downstream of the element, no effect of the roughness element on the pressure distribution was detected.

Recovery-Factor Distributions

Without roughness elements. - Recovery-factor distributions corresponding to the test conditions of figure 2 are presented in figure 3. Temperature-recovery factor η is defined by the equation

$$\eta = \frac{T - T_\infty}{T_0 - T_\infty}$$

(Symbols are defined in appendix A.) For the cylinder without a roughness element (fig. 3(a)), the recovery factors nearest the leading edge

range between 0.854 and 0.857, which are quite close to the theoretical laminar value of about 0.850 obtained from the Prandtl number evaluated at the measured recovery temperature. In reference 2 the corresponding recovery factors measured were 0.867 to 0.878.

The reason for this reduction in initial recovery factor in the present investigation is believed to be associated with the reduction in leading-edge thickness. Reference 4 found that the experimental laminar-boundary-layer profiles approached the theoretical as the leading-edge thickness was reduced. By analogy, this tendency might be expected to hold for the measured recovery factors also and thus account for the improved agreement between experiment and theory in the present instance compared with that noted in reference 2.

A further comparison of figure 3(a) with the recovery factors presented in reference 2 indicates a forward shift in the present recovery-factor peaks for corresponding values of free-stream Reynolds number per inch. If the transition points are taken to be at the temperature peak, as in reference 2, this forward shift is equivalent to a reduction in transition Reynolds number.

The turbulent recovery factors, which correspond to the more or less horizontal distribution of points to the right of the peaks in figure 3(a), agree fairly well with those obtained in reference 2. The values lie between 0.875 and 0.886 and show the same characteristic variation with U_∞/ν_∞ as observed in reference 2. Theoretical turbulent recovery factors as given in reference 5 for the present test conditions are very close to 0.885. These are based on a temperature that is the arithmetic mean of the measured turbulent recovery temperature and the free-stream static temperature.

Recovery-factor distributions for the cylinder used in the present tests, the cylinder of reference 2, and the cone of reference 1 are compared in figure 4 for values of U_∞/ν_∞ of 3.5 and 6.7×10^5 per inch. These models were all tested in the same wind tunnel, and the recovery factors have been interpolated to the same Reynolds number per inch. Recovery factors and Reynolds numbers for the cone are based on local conditions outside the boundary layer where the Mach number was 3.0. The effect of such a small difference in local Mach number on the laminer-boundary-layer stability has been neglected in the present analysis in the interest of simplicity, according to figure 11 of reference 6. Since the skin thicknesses in all cases were the same, differences in the recovery-factor distributions should reflect differences in external model geometry only.

Recovery factors in the laminar region are lowest for the cone and highest for the cylinder of reference 2 having the 0.006-inch-thick leading edge. Transition locations x_t, given by temperature peaks in the

recovery-factor distributions, are lowest for the present cylinder having the 0.0008-inch-thick leading edge and highest for the cone of reference 1. The ratio of the cone to the cylinder transition Reynolds number is 2.4 and 1.7 for U_∞/ν_∞ of 3.5 and 6.7×10^5, respectively, whereas from stability theory the value suggested by reference 6 (p. 803) is 3. For the cylinder of reference 2 having the 0.006-inch-thick leading edge, this ratio is 1.2 and 1.4 for the same values of U_∞/ν_∞, respectively. Thus, by increasing the sharpness of the cylinder (or flat plate) leading edge, transition Reynolds numbers are reduced and the ratio of the cone to the cylinder transition Reynolds number is brought into closer agreement with the predictions of stability theory. By this means also, experimental laminar recovery factors for the cylinder are made to approach the theoretical values. Because of the slight heat transfer through the leading edge of the cylinder (this problem was treated theoretically in ref. 7), or the difficulty in obtaining a sufficiently sharp leading edge, it may be impossible to reach the low initial recovery factors found on a cone, however.

3464

With roughness elements. - The effect of the size of a single roughness element on the recovery-factor distribution may be seen in figures 3(b) to (d). In these figures the distance of the element from the leading edge x_k was 12 inches, and the roughness elements were 0.010, 0.032, and 0.079 inch high, respectively. The effect of roughness-element location, on the other hand, is illustrated in figures 3(c), (e), (f), and (g), where the element size was 0.032 inch and its position x_k was 12, 8, 4, and 2 inches downstream of the leading edge, respectively.

When the roughness elements were located at $x_k = 12$ inches, they were in the turbulent boundary layer for the three highest values of Reynolds number per inch and at the transition point for the lowest value. The recovery-factor distributions show little change from the distributions of figure 3(a) in the initial 10 inches from the leading edge. An exception to this behavior occurs in figure 3(b) for the 0.010-inch element, where the transition point is displaced upstream slightly. This discrepancy was caused by a slight variation in the sharpness of the leading edge and is independent of the roughness-element size; in no instance did the roughness elements have any effect on the transition-point location for $x_k = 12$ inches.

In the remaining figures (3(e) to (g)), the 0.032-inch roughness element was located in the laminar, transitional, and turbulent regions of the boundary layer. Examination of the various parts of figure 3 reveals the following characteristics of the recovery-factor distributions: For an element in the laminar boundary layer, no abrupt perturbation of the recovery temperature near the element can be detected; only a slight upstream shift of the transition point takes place. When the element is placed in the turbulent layer, large perturbations in the temperature distribution result, with no effect on the transition-point

location. If the element is placed near the transition point, then the temperature rise associated with transition and that caused by the element in the turbulent boundary layer become superimposed, resulting in the highest surface temperatures observed.

Temperature variations caused by the element in the turbulent boundary layer were greatest for the largest roughness elements. The highest values of the surface temperature, whether caused by transition, by a roughness element in the turbulent boundary layer, or by a combination of the two, always occurred at the lowest tunnel Reynolds number. The lowest values of surface temperature downstream of an element in the turbulent or transitional boundary layer occurred at the highest tunnel Reynolds number. In general, deviations in turbulent recovery factor caused by the roughness elements tended to wash out downstream on the model where the turbulent recovery factors approached those obtained without roughness. Evidence of this wash-out for the most severely perturbed turbulent recovery factor is apparent from a comparison of figures 3(d) and (a).

High-Speed Schlieren Motion Pictures

High-speed schlieren motion pictures having a 16:1 magnification normal to the stream direction were taken of the boundary layer with and without roughness at the various test conditions used in figure 3. A typical enlargement of a single frame taken at a Reynolds number of 1.82×10^5 per inch without a roughness element is shown in figure 5. This photograph was taken at a film speed of 4000 frames per second, giving an individual frame exposure of about 1/12,000 second. This exposure is about 100 times longer than that attainable with the short-duration spark sources commonly used for high-speed schlieren photographs; and, consequently, some of the very high-speed movements appear blurred and cannot be distinguished in the example shown. This loss of detail in the individual frames is partly compensated for in viewing the film with a conventional motion-picture projector, however. Much of the succeeding description is based on observations of the projected motion pictures and is not detectable on the single-frame photograph of figure 5. The slight bend in the cylinder surface is caused by the magnification of a much smaller bend (0.020 in. in 18 in. of length) in the actual cylinder.

In figure 5 the light streak adjacent to the model surface, which is identified as the laminar boundary layer, appeared to be completely steady, except for the lowest value of U_∞/ν_∞, where slight undulations of the laminar boundary layer were apparent. This length of laminar run corresponds with the distance from the leading edge to a point somewhat upstream of the peak recovery temperature for each value of Reynolds number per inch, as is indicated in figure 3(a).

Immediately following the steady laminar flow, a region of comparatively violent fluctuations appeared. Because the picture was distorted by the unilateral magnification of the schlieren system and because of the lack of sufficient speed and resolution in the motion-picture camera, the interpretation of the movements observed is not entirely clear; for example, some observers maintained that the fluctuations could resemble a fore and aft motion of the transition point, whereas others claimed that the picture was one of intermittent separation and reattachment of the laminar boundary layer. Whether either or both of these explanations are an adequate description of the physical phenomena can be ascertained only by further experimentation. These observations, crude as they may be, confirm the general notion that the transition from laminar to turbulent flow requires some distance to take place and is accompanied by rather violently fluctuating movements. The length of this fluctuating region, which was measured from the projected image, varied between 1.5 and 6 or more inches as Reynolds number was reduced from 6.61 to 0.95×10^5 per inch. These regions are indicated in figure 3(a). The Reynolds number based on the length of this transition region varies between 6×10^5 and 10×10^5.

The edge of the turbulent boundary layer was not as well defined as that of the laminar; and often the only evidence of its outer extremity was a random fluctuating motion, appreciably less violent than in the transition region. This motion was visible to the downstream extremity of the schlieren field of view.

Transition Reynolds Number

The transition points, defined as the temperature-peak locations along the surface, and the transition Reynolds numbers, without roughness, were found as a function of free-stream Reynolds number. These results (figs. 6 and 7) were obtained at two positions in the tunnel test section 3.3 inches apart, as described in the test procedure. Comparison of the data shows that there is little if any effect of model location in the test section for the two positions tested. Most of the differences between the two sets of data are believed resolvable in terms of erosion and wear of the leading edge. The same explanation would apply to the slight differences in temperature-peak locations of figures 3(a) and 6.

Two of the curves in figure 7 were obtained by the equation

$$Re_t = D\sqrt{U_\infty/\nu_\infty}$$

which was used to correlate the zero-roughness results found in reference 2. The constant D is estimated from the present results to be

about 2900, whereas reference 2 showed it to be 5000. If a more general relation for the transition Reynolds number of the type

$$Re_t = D\left(\frac{U_\infty}{\nu_\infty}\right)^m \tag{1}$$

is assumed, a curve described by the expression

$$Re_t = 12{,}300\left(\frac{U_\infty}{\nu_\infty}\right)^{0.39}$$

is found to fit the present experimental results better than the square-root relation (fig. 7). The large discrepancy between the present correlation of the transition Reynolds number with U_∞/ν_∞ and that obtained in reference 2 is caused by the differences in leading-edge thickness for the two model configurations.

Heat-Conduction Effects

Near transition region. - The gradual rise in recovery temperature along a cone from a laminar to a turbulent value was correlated in reference 1 with a random movement of the transition point observed by means of high-speed schlieren photography. A succeeding investigation (ref. 2) showed the recovery-temperature rise measured on a cylinder to be much flatter than on the cone, and yet the random movement of the transition point observed with high-speed photography had a relatively short extension, comparable with that observed for the cone. Hence, in reference 2 the random transition-point movement could not account for the relatively flat surface temperature distribution on the cylinder. An explanation for the very gradual temperature rise was then sought in possible heat-conduction effects through the cylinder skin. The effect of conduction on the surface temperature was computed and was found to be much smaller than required to produce the observed temperature distribution.

In the present experiment the temperature variations along the cylinder are considerably more abrupt than reported in reference 2, and conduction effects have consequently been reassessed. The method used to calculate the conduction effects and the assumptions involved are presented in appendix B. The results of the calculations and a comparison with experiment are presented in figure 8 for four values of Reynolds number per inch. The ordinate θ is a dimensionless temperature resulting from the solution of the differential equation for the heat flow and is defined as

$$\theta = \frac{T - T_{ad}}{T_f - T_{ad}}$$

where T_{ad} is the laminar recovery temperature assumed to hold at the leading edge, and T_f is a fixed wall temperature occurring at the end of the laminar region as described in appendix B. Experimental values of θ were computed using for T_{ad} the temperature at the first thermocouple and for T_f the temperature at the end of the steady laminar region shown in figure 3(a).

Figure 8 indicates that the computed temperature distributions which consider only shell conduction effects vary appreciably from the experimental distributions. These variations suggest that the heat-transfer rates given by reference 8 are too low to produce the more gradual temperature rises observed experimentally. This is particularly true of the lowest Reynolds number and to a lesser extent of the others. For the lowest Reynolds number, undulations in the laminar boundary layer were clearly perceptible from the motion-picture studies, as was pointed out earlier, and may have increased the heat transfer above the steady-state laminar value assumed in the computations. Although such undulations were not strong enough to be apparent at the higher Reynolds numbers, it is conceivable that they existed and had a similar but smaller effect on the experimental temperature distributions. It may be concluded that steady-state heat-conduction effects account for an appreciable part of the temperature rise ahead of the transition point, but they do not account for it entirely.

The drop in the recovery factor following the peak (fig. 3) is probably representative of a gradual diminution of the mixing action throughout the transition region to a magnitude characteristic of the turbulent flow. In such a region heat-conduction effects would be extremely difficult to evaluate, since heat-transfer coefficients for the transition region are not known. If it is granted that these coefficients are considerably greater than the laminar ones, then in all probability the temperature drop after the peak is not appreciably influenced by conduction of heat in the cylinder skin.

Near roughness elements. - The previous discussion of the temperature rise at the roughness element did not consider possible effects of heat conduction within the cylinder surface in the neighborhood of the element. A calculation of the temperature distribution based on the method given in appendix B using turbulent heat-transfer coefficients also indicates an appreciable upstream influence of conduction on the surface temperature. It may therefore be assumed that the temperature rise which would exist in the absence of surface conduction would be higher and more abrupt than shown in figure 3.

The temperature rise following the temperature undershoot downstream of the element is too gradual to be explainable in terms of the preceding conduction analysis. In the case of the 0.079-inch element of figure 3(d), for example, the surface temperature rose slowly for a distance of 14 inches before reaching the value attained without a roughness element.

Qualitative Description of Observed Flows

Based on the high-speed schlieren motion pictures, instantaneous spark schlieren photographs, surface temperature distributions, and analyses of the conduction effects, a unified picture of boundary-layer transition and the effect of single roughness elements can be formulated. A sketch of the boundary-layer transition without roughness is presented in the lower portion of figure 9(a), and the corresponding temperature distribution is shown above. The steady laminar-boundary-layer run observed in the motion pictures terminates slightly ahead of the temperature peak. Here a transition region is initiated in which large random disturbances or fluctuations are formed that finally develop into a turbulent boundary layer, having a diffuse outer edge and smaller random oscillations. The term "transition region" applies to the region of large fluctuations designated in figure 3(a), whereas the term "transition point" identifies the location of the peak temperature within the transition region.

The corresponding surface temperature distribution indicates an initial recovery temperature somewhat higher than the theoretical laminar value, which may be accounted for by either or both of the following explanations: (1) conduction and convection of heat in a downstream direction from the interior of the leading edge; (2) error in computing the recovery factor because the actual velocity at the edge of the boundary layer is less than free stream because of the shock losses near the leading edge. As the leading-edge effect washes out, the temperature drops slightly, reaches a minimum, and begins to rise in the steady laminar flow region. A significant part of this premature rise may be explained, at least for the high Reynolds numbers, as forward conduction of heat within the model skin from the high-temperature source occurring at the transition point. If this explanation for the temperature rise is granted, then the temperature rise that would occur in the absence of conduction will become more abrupt. The temperature peak apparently is associated with a violent mixing action, and the decrease in wall temperature with increasing downstream distance is the result of attenuation of mixing to a value characteristic of the turbulent boundary layer.

When the roughness element is placed in the laminar boundary layer, the schlieren photographs present an appearance similar to figure 9(b). The roughness element at x_k causes a separation ahead of the element with an attendant gradual compression of the flow. This gradual compression takes place through a system of Mach waves that coalesce and form a weak compression shock several element heights away from the surface. An expansion fan is produced as the flow turns around the top of the element, the flow becomes overexpanded, and a second shock compresses the flow to the free-stream value again. Most of the details of the shock structure shown in figures 9(b) and (c) were obtained from

an examination of a large number of undistorted instantaneous (3-microsec) schlieren photographs where roughness-element size and location and Reynolds number covered the full range of the experimental conditions reported in reference 2.

At some distance downstream of the element and close to the surface, the motion pictures showed small disturbances forming in the laminar boundary layer. These were swallowed up in the large-scale fluctuations at the start of the transition region, and the flow from here on appeared the same as in figure 9(a), except that the transition point was shifted upstream somewhat. No temperature perturbation occurred in the neighborhood of the element when it was placed in the laminar boundary layer.

When the element was moved into the turbulent region of the flow (fig. 9(c)), the picture appeared very similar to that without roughness, except that a shock-expansion-shock wave formed off the element. In distinction to the shock formation of figure 9(b), that of figure 9(c) showed both of the shock waves penetrating to the model surface; that is, the initial gradual compression region was absent. The surface temperature followed the distribution obtained with zero roughness up to a point near the roughness element, where a sudden rise and fall in temperature occur. From the earlier conduction analysis, it may be presumed that the temperature rise at the element in the absence of surface conduction would be steeper and higher than shown. The region of minimum recovery temperature immediately downstream of the roughness element extends many diameters downstream of the wire and consequently is not directly associated with the overexpansion around the wire.

SUMMARY OF RESULTS

From a study of surface temperature distributions for an insulated cylinder at Mach 3.12 with and without single roughness elements and of simultaneous high-speed schlieren motion pictures, the following results were obtained:

1. With no roughness element present, the recovery factor in the laminar boundary layer was reduced as the leading edge was sharpened (from 0.006- to 0.0008-in. thickness) and approached the theoretical value as a lower limit. Sharpening the leading edge produced an upstream displacement of the recovery-factor peak and hence a corresponding displacement of the transition-point location, and a closer resemblance to the recovery-factor distribution observed on a cone.

2. With no roughness element present, the high-speed schlieren motion pictures showed the boundary layer to be laminar almost to the peak in the recovery-factor distribution. At this point, violent fluctuation of the boundary layer took place, continuing until a relatively

stable turbulent boundary layer was established. This fluctuating region corresponded to the transition region and was found to increase in length as the stream Reynolds number per inch was reduced.

3. The surface temperature distribution in the neighborhood of a single roughness element depends on the type of boundary layer at the element. For an element in the laminar boundary layer, very slight temperature rises ahead of the element and an upstream movement of the recovery temperature peak (and hence of the transition point) were noted. For an element in the turbulent boundary layer, a relatively large abrupt rise in temperature immediately ahead of the element and a sharp drop after the element were observed. For an element in the transition region, the temperature rise associated with the element accentuated the temperature rise at the transition point.

Lewis Flight Propulsion Laboratory
National Advisory Committee for Aeronautics
Cleveland, Ohio, May 9, 1955

APPENDIX A

SYMBOLS

The following symbols are used in this report:

a_n	numerical constant
C	viscosity-temperature proportionality factor (ref. 8)
C_p	pressure coefficient, $2(p - p_\infty)/\rho_\infty U_\infty^2$
D	numerical constant
$J_{2/3}$	2/3-order Bessel function
K	constant defined by eq. (B5)
k_s	thermal conductivity of surface material
k_∞	thermal conductivity of air in free stream
m	exponent in transition Reynolds number correlation, eq. (1)
n	exponent in temperature distribution, eq. (B3)
p	static pressure
q	heat flow per unit width of surface
Re	Reynolds number, $U_\infty x/\nu_\infty$
T	absolute temperature
t	thickness of conducting surface
U	velocity
x	axial distance
$Y_n'(0)$	function defined in ref. 8
y	variable defined by eq. (B8)
z	variable defined by equation $\xi = z^2$
η	temperature-recovery factor, $(T - T_\infty)/(T_0 - T_\infty)$

θ dimensionless temperature, $(T - T_{ad})/(T_f - T_{ad})$

ν kinematic viscosity

ξ dimensionless distance, x/x_f

ρ mass density

Subscripts:

ad adiabatic laminar value

f downstream extremity of steady laminar boundary layer

k condition at roughness element

t conditions at transition point

0 stagnation condition

∞ property or condition in free stream

APPENDIX B

ANALYSIS OF WALL CONDUCTION EFFECTS

In determining the magnitude of the conduction effects within the thin outer shell, it is assumed that in the absence of conduction an ideal temperature distribution exists, as indicated by the dotted line in sketch (a):

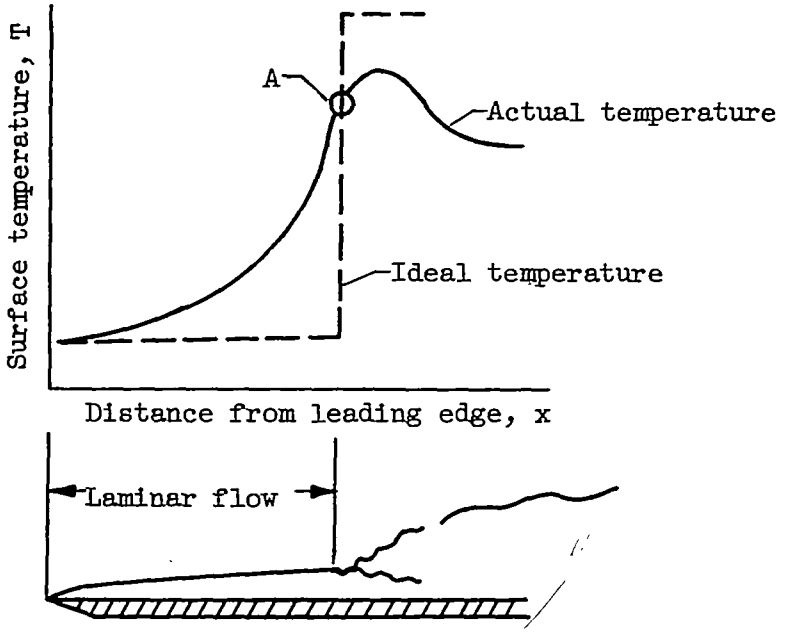

Sketch (a)

The following analysis will suggest whether surface conduction effects might so modify the ideal temperature distribution as to make it coincide with the actual temperature distribution indicated by the solid line in the laminar region.

Consider the temperature distribution in the laminar-flow region upstream of the inflection point A in sketch (a). In this region the wall will be taken as a conducting shell that terminates at the inflection point and has a fixed temperature T_f imposed on the terminal edge x_f shown in sketch (b):

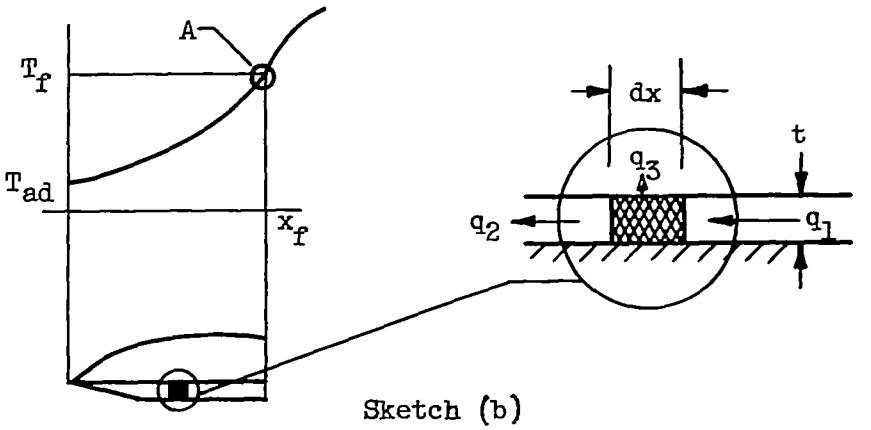

Sketch (b)

Fluctuations in transition-point location upstream of x_f are assumed negligible in this analysis. The temperature at the leading edge is taken as the laminar recovery temperature T_{ad}, and the underside of the shell is insulated. The upper surface is assumed to be completely in the laminar-flow region.

A heat balance may be written by considering the heat flow in a section of the plate, which is shown enlarged on the right in sketch (b):

$$q_1 = q_2 + q_3 \tag{B1}$$

where q is the heat flow per unit width of section and is given by

$$\left.\begin{aligned} q_1 &= tk_s \frac{dT}{dx} \\ q_2 &= tk_s \left(\frac{dT}{dx} + \frac{d^2T}{dx^2}\,dx\right) \\ q_3 &= -\frac{k_\infty T_\infty}{2}\sqrt{\frac{U_\infty C}{\nu_\infty x}}\, a_n \left(\frac{x}{x_f}\right)^n Y_n'(0)\,dx \end{aligned}\right\} \tag{B2}$$

The last expression $Y_n'(0)$ is obtained from equation (50) of reference 8 when the wall temperature is represented by the simple power relation:

$$\frac{T - T_{ad}}{T_\infty} = a_n \left(\frac{x}{x_f}\right)^n \tag{B3}$$

and the viscosity-ratio factor C is taken for a constant wall temperature. The function $Y_n'(0)$ is tabulated against n in reference 8.

Substitution of equations (B3) into (B2) and (B2) into (B1) gives the differential heat-balance equation

$$\frac{d^2T}{dx^2} - \frac{Y_n'(0)\, k_\infty}{2\, tk_s}\sqrt{\frac{U_\infty C}{\nu_\infty x}}\,(T - T_{ad}) = 0 \tag{B4}$$

with the boundary conditions

$$T(0) = T_{ad}$$

$$T(x_f) = T_f$$

Equation (B4) can be nondimensionalized by introduction of the new variables $\theta = (T - T_{ad})/(T_f - T_{ad})$ and $\xi = x/x_f$, resulting in the equation

$$\frac{d^2\theta}{d\xi^2} - K\frac{\theta}{\sqrt{\xi}} = 0$$

where

$$K = \left(\frac{Y_n'(0)}{2}\right)\frac{k_\infty}{k_s}\frac{x_f}{t}\sqrt{Re_f C} \tag{B5}$$

The boundary conditions become

$$\theta(0) = 0$$

$$\theta(1) = 1$$

Equation (B5) may be transformed into Bessel's equation by introducing the new variable z, where $\xi = z^2$. Thus,

$$z^2\frac{d^2\theta}{dz^2} - z\frac{d\theta}{dz} - 4Kz^3\theta = 0 \tag{B6}$$

with the boundary conditions $\theta(0) = 0$ and $\theta(1) = 1$.

A solution of equation (B6) is given in reference 9 (pp. 438 to 440). After applying the above boundary conditions, the solution may be written as

$$\theta = \frac{zJ_{2/3}\left(\frac{2}{3}\sqrt{-4K}\,z^{3/2}\right)}{J_{2/3}\left(\frac{2}{3}\sqrt{-4K}\right)} \tag{B7}$$

Tabulated values for the 2/3-order Bessel functions with imaginary argument are given in reference 10. For values of the argument greater than those included in reference 10, the following asymptotic formula gives sufficient accuracy for the present purposes:

$$i^{-2/3}J_{2/3}(iy) = \sqrt{\frac{1}{2\pi}}\frac{e^y}{\sqrt{y}}$$

where

$$iy = \frac{2}{3}\sqrt{-4K}\,z^{3/2} \tag{B8}$$

Values of K were obtained from a knowledge of the Reynolds number, the distance x_f, and the shape of the experimental temperature distribution. It was assumed that the experimental temperature distribution could be adequately represented by the power relation of equation (B3), which in turn made it possible to determine $Y_n'(0)$. Values of x_f, n, $Y_n'(0)$, and K used in the present calculations are as follows:

U_∞/ν_∞ per in.	x_f, in.	n	$Y_n'(0)$	K
6.61×10^5	3.4	5.5	1.645	76.5
3.48	4.9	5.5	1.645	96.0
1.82	6.4	5.5	1.645	103.7
.95	10.4	3.3	1.400	132.2

A plot of the wall temperature distribution θ against ξ given by equation (B7) is presented in figure 8 for the listed values of K. Comparison of the computed and experimental temperature distributions indicates that heat-transfer effects in excess of those given by the theory of reference 8 very likely are present. These may be caused by fluctuations in the transition-point location or possibly by unsteady motions in the laminar boundary layer.

REFERENCES

1. Evvard, J. C., Tucker, M., and Burgess, W. C., Jr.: Statistical Study of Transition-Point Fluctuations in Supersonic Flow. NACA TN 3100, 1954.

2. Brinich, Paul F.: Boundary-Layer Transition at Mach 3.12 with and without Single Roughness Elements. NACA TN 3267, 1954.

3. Buchele, D. R., and Goosens, H. R.: Lens System Producing Unequal Magnification in Two Mutually Perpendicular Directions. Rev. Sci. Inst., vol. 25, no. 3, Mar., 1954, pp. 262-263.

4. Brinich, Paul F., and Diaconis, Nick S.: Boundary-Layer Development and Skin Friction at Mach Number 3.05. NACA TN 2742, 1952.

5. Tucker, Maurice, and Maslen, Stephen H.: Turbulent Boundary-Layer Temperature Recovery Factors in Two-Dimensional Supersonic Flow. NACA TN 2296, 1951.

6. Van Driest, E. R.: Calculation of the Stability of the Laminar Boundary Layer in a Compressible Fluid on a Flat Plate with Heat Transfer. Jour. Aero. Sci., vol. 19, no. 12, Dec. 1952, pp. 801-812.

7. Korobkin, Irving: Apparent Recovery Factors on the Leading Edge of a Flat Plate in Supersonic Laminar Flow. Jour. Aero. Sci., vol. 20, no. 8, Aug. 1953, pp. 578-579.

8. Chapman, Dean R., and Rubesin, Morris W.: Temperature and Velocity Profiles in the Compressible Laminar Boundary Layer with Arbitrary Distribution of Surface Temperature. Jour. Aero. Sci., vol. 16, no. 9, Sept. 1949, pp. 547-565.

9. Kamke, E.: Differentialgleichungen. Akad. Verlagagesellschaft, Becker & Erler Kom. -Ges. (Leipzig), 1943, pp. 437-450.

10. Jahnke, Eugene, and Emde, Fritz: Tables of Functions. Fourth ed., Dover Pub., 1945, p. 235.

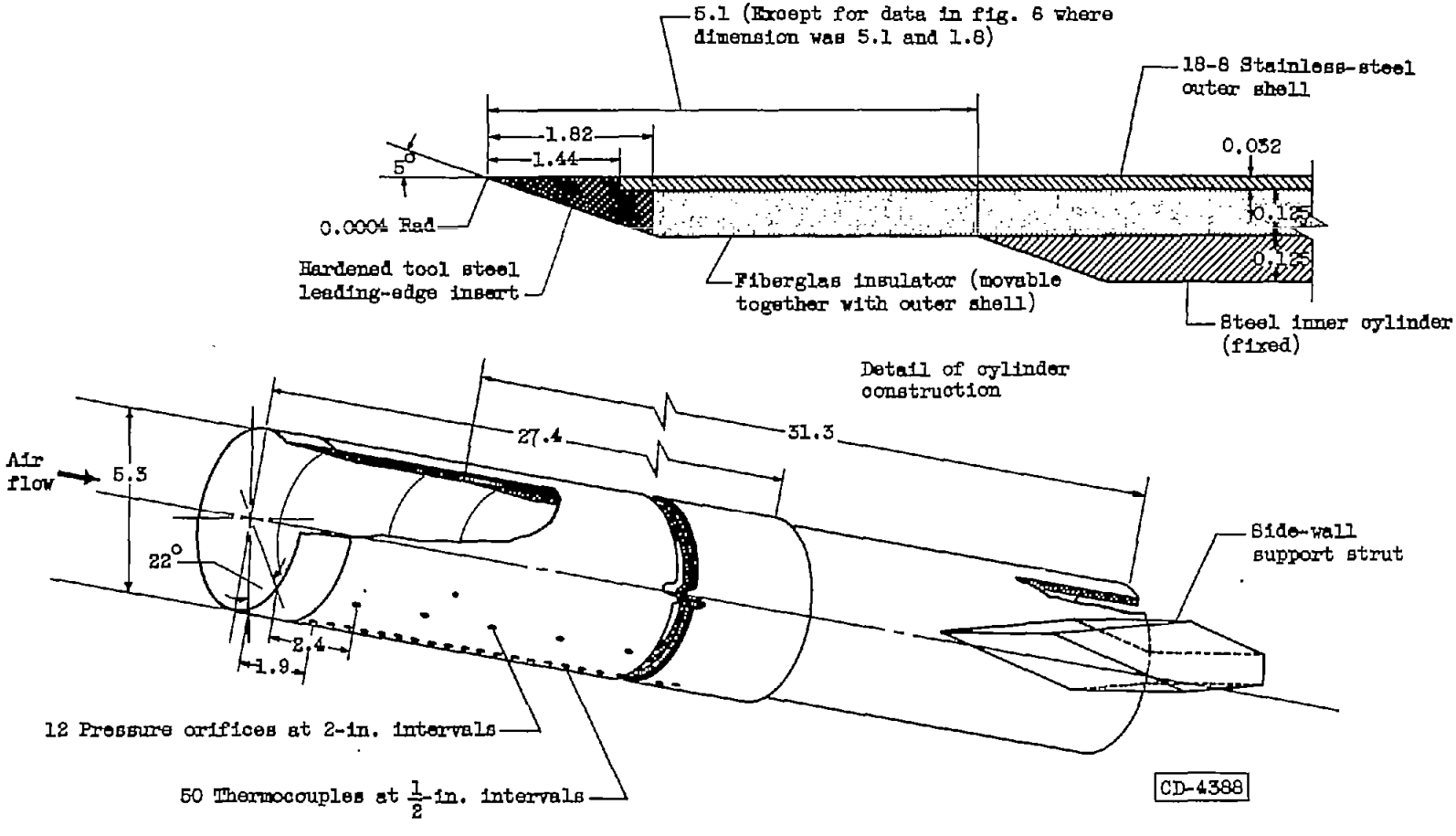

Figure 1. - Cylinder model used in investigation. (All dimensions in inches.)

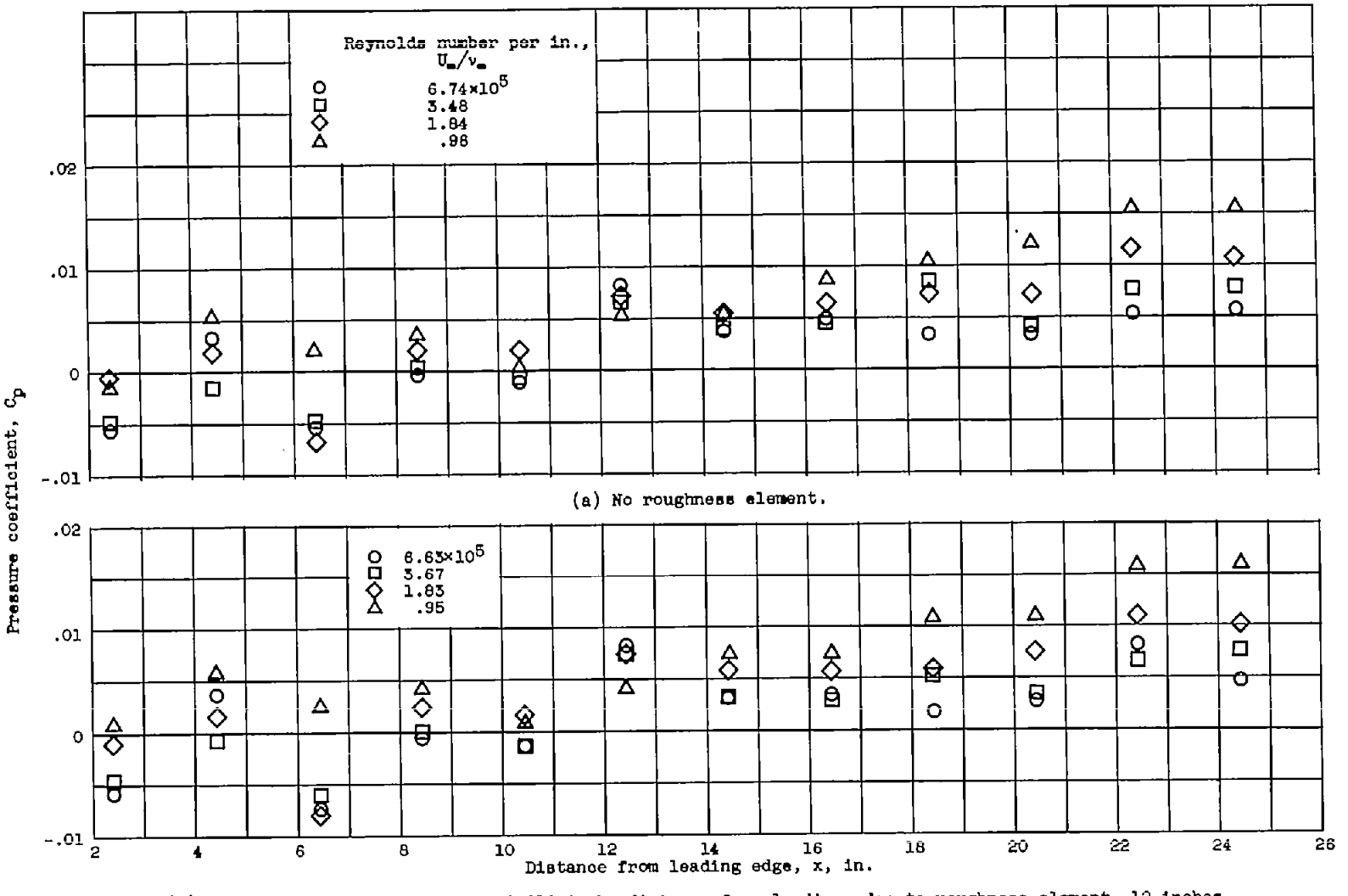

(b) Height of roughness element, 0.010 inch; distance from leading edge to roughness element, 12 inches.

Figure 2. - Pressure-coefficient distributions at various free-stream Reynolds numbers.

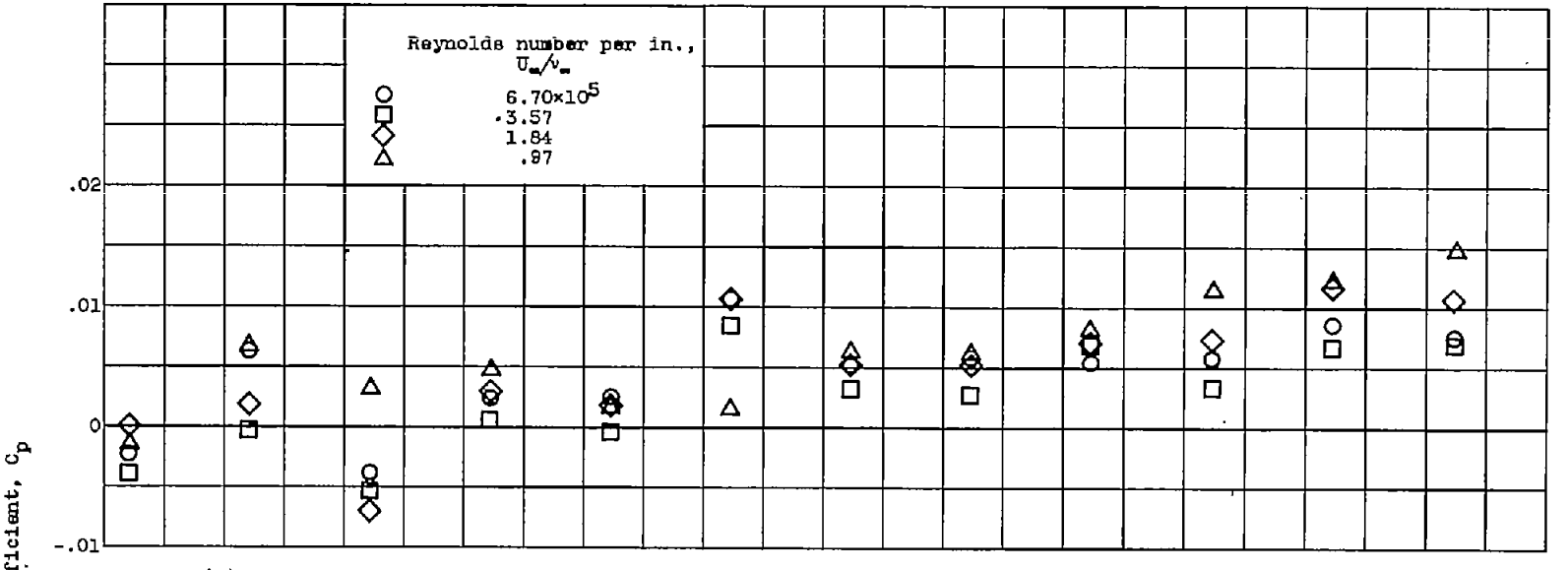

(c) Height of roughness element, 0.032 inch; distance from leading edge to roughness element, 12 inches.

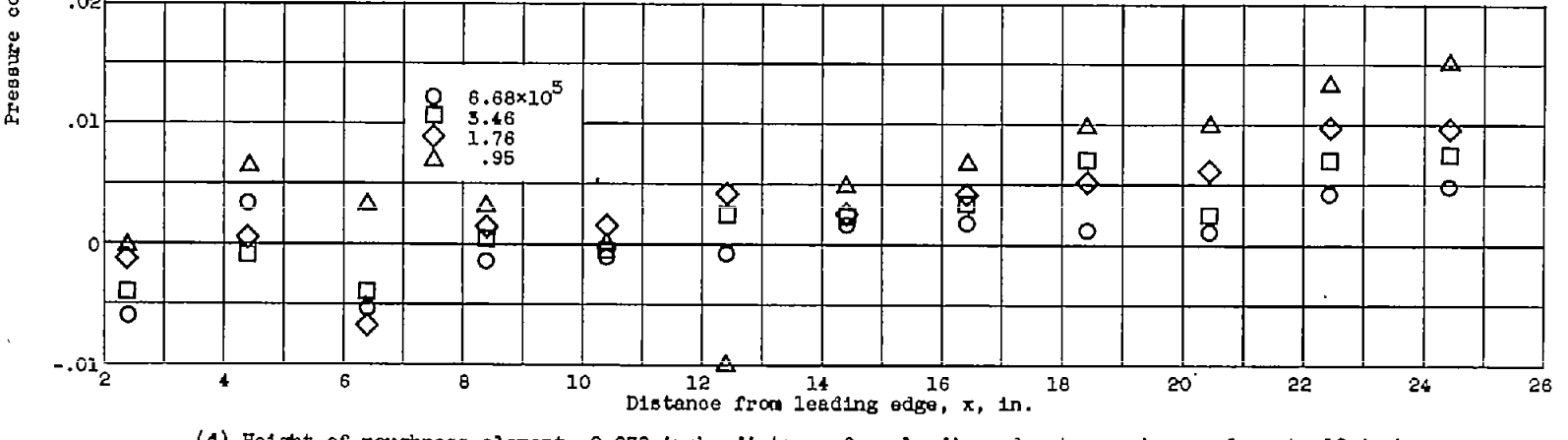

(d) Height of roughness element, 0.079 inch; distance from leading edge to roughness element, 12 inches.

Figure 2. - Continued. Pressure-coefficient distributions at various free-stream Reynolds numbers.

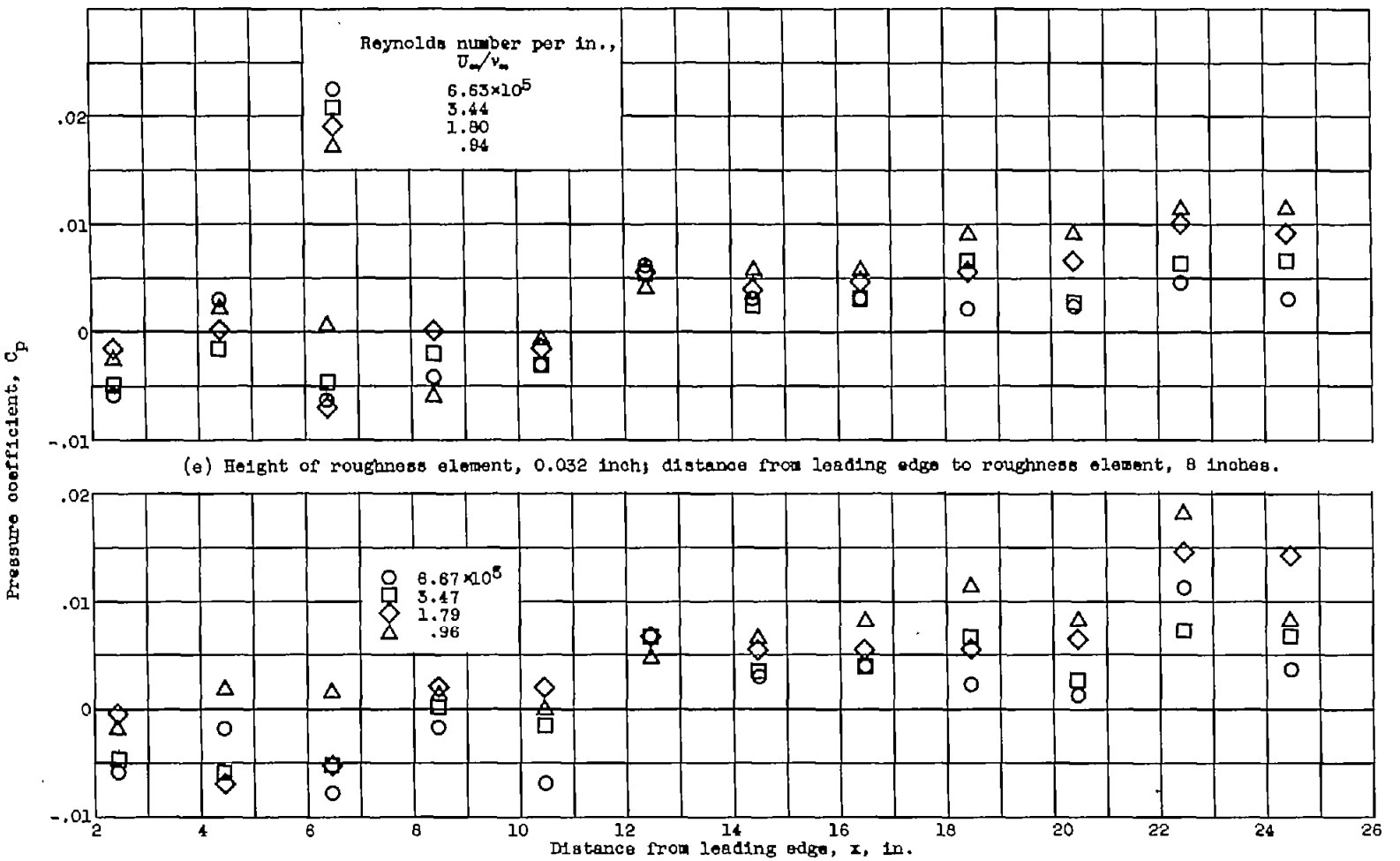

(e) Height of roughness element, 0.032 inch; distance from leading edge to roughness element, 8 inches.

(f) Height of roughness element, 0.032 inch; distance from leading edge to roughness element, 4 inches.

Figure 2. - Continued. Pressure-coefficient distributions at various free-stream Reynolds numbers.

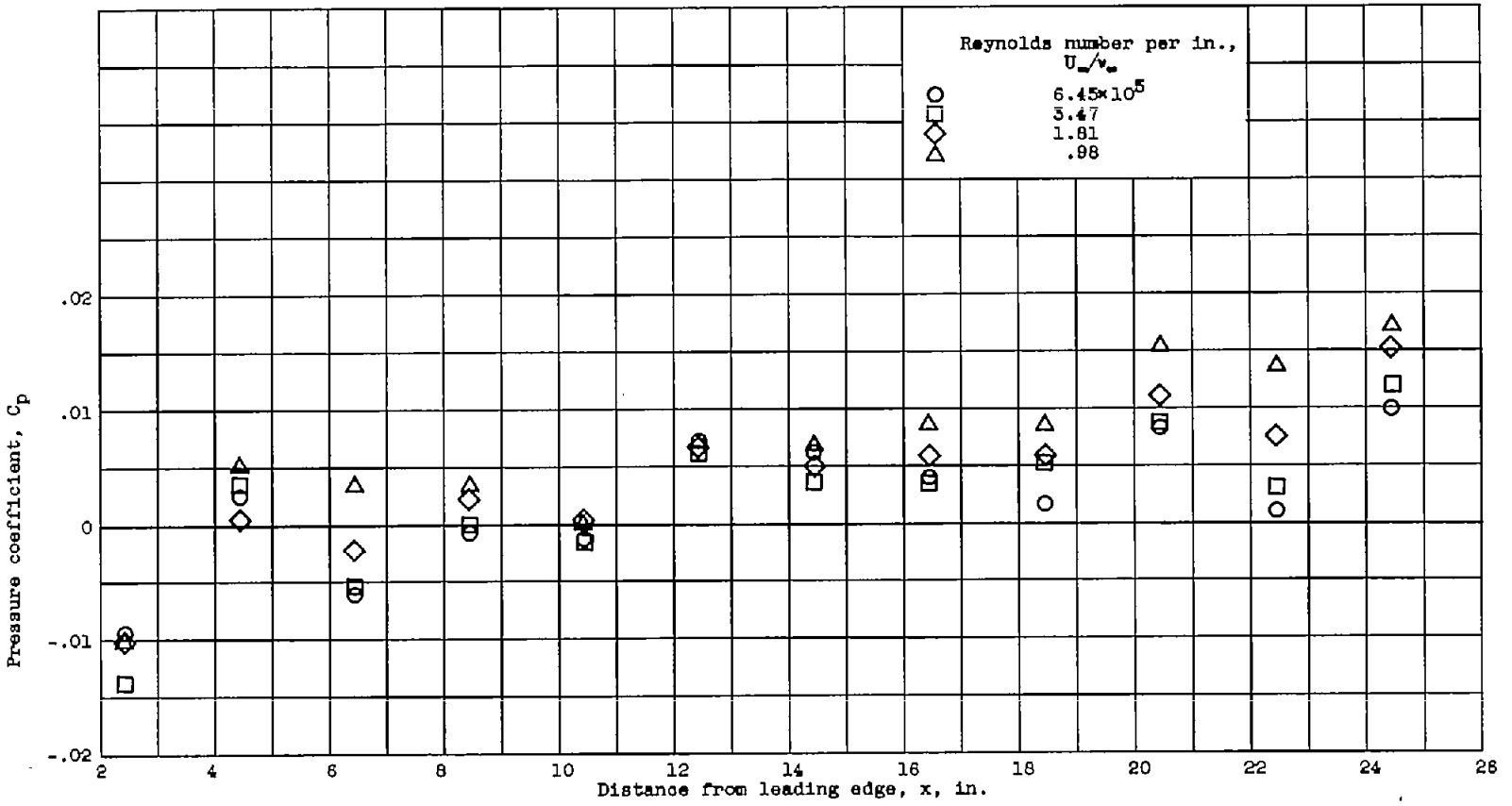

(g) Height of roughness element, 0.032 inch; distance from leading edge to roughness element, 2 inches.

Figure 2. - Concluded. Pressure-coefficient distributions at various free-stream Reynolds numbers.

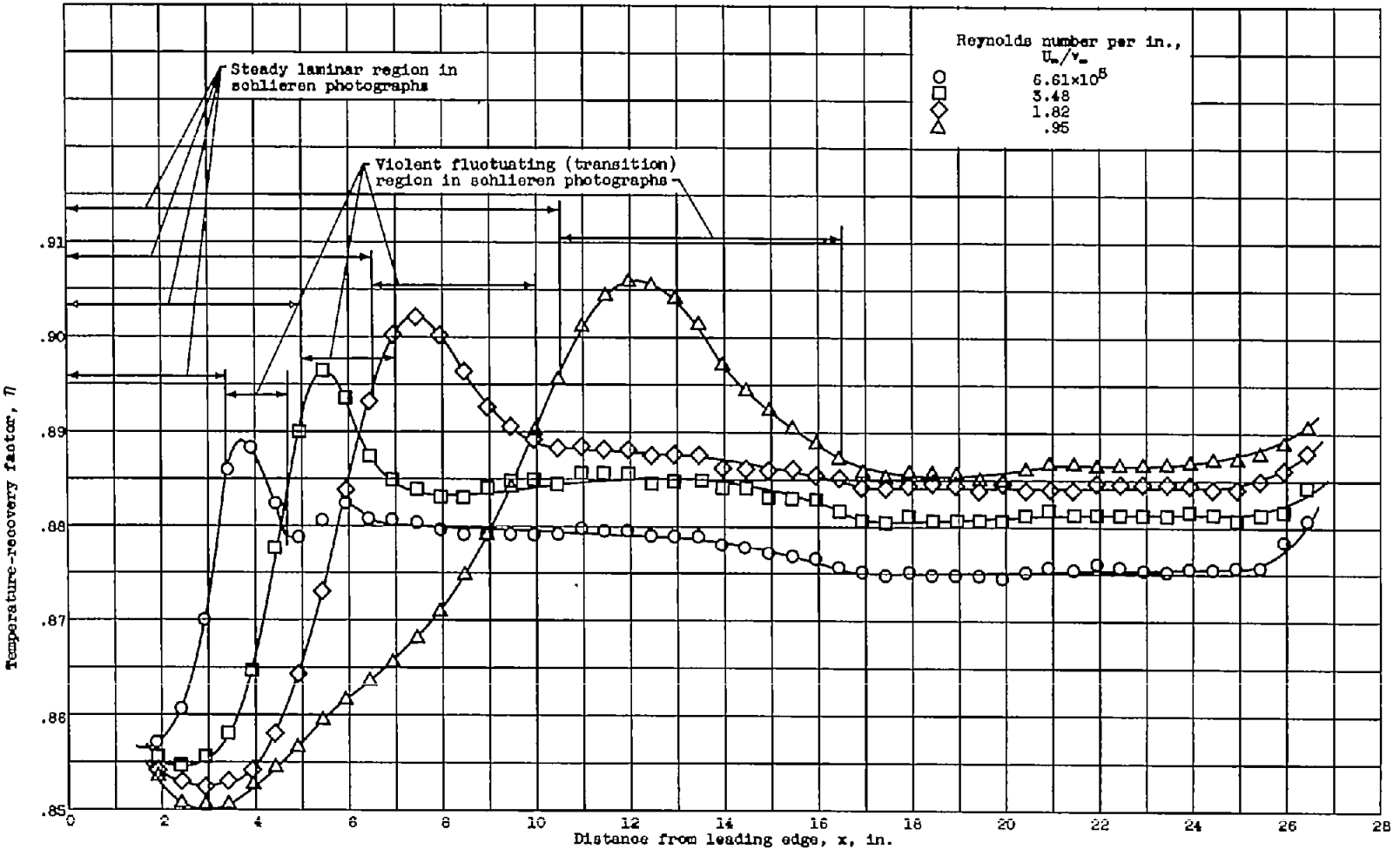

(a) No roughness element.

Figure 3. - Recovery-factor distributions at various free-stream Reynolds numbers.

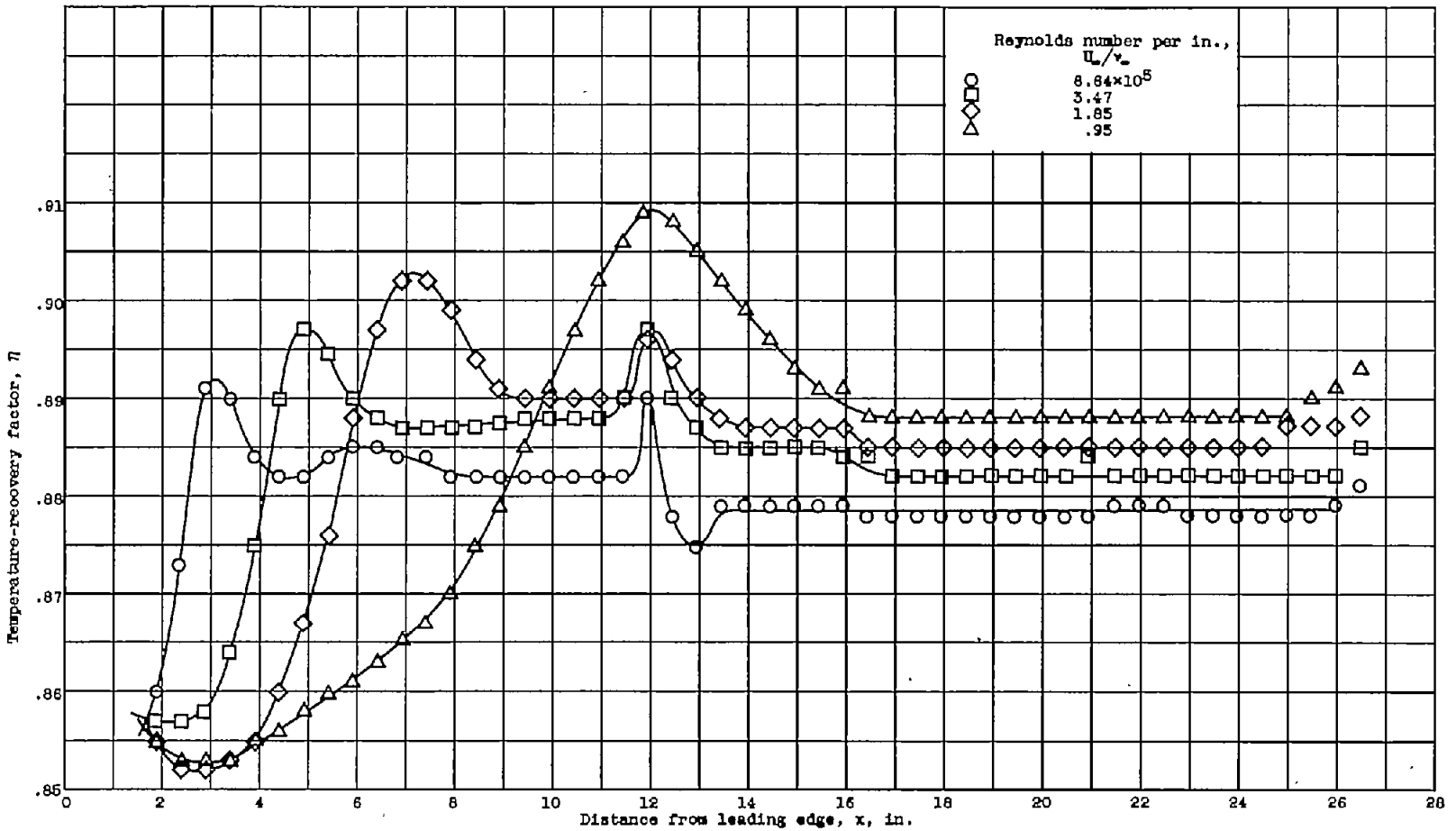

(b) Height of roughness element, 0.010 inch; distance from leading edge to roughness element, 12 inches.

Figure 3. - Continued. Recovery-factor distributions at various free-stream Reynolds numbers.

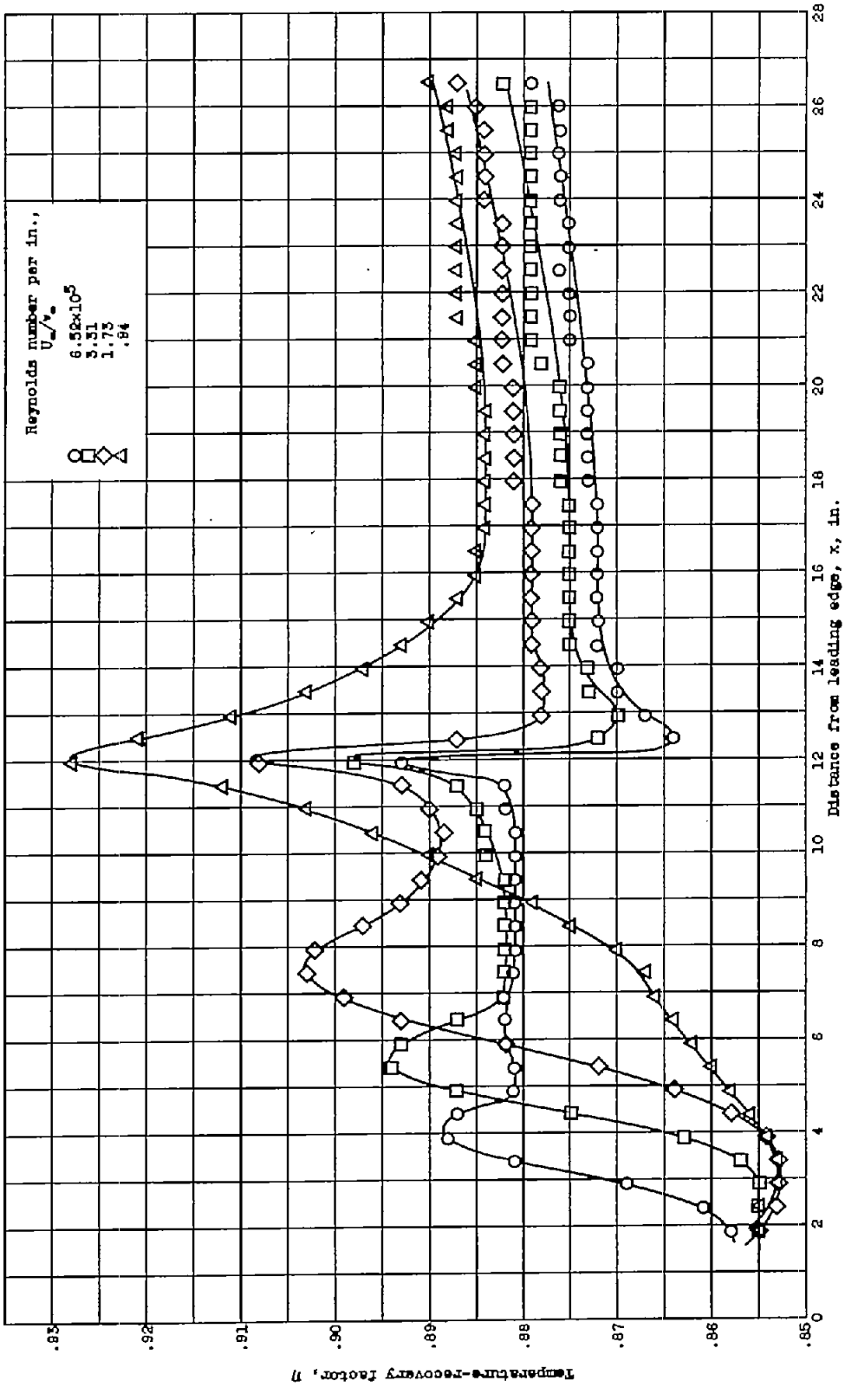

(c) Height of roughness element, 0.052 inch; distance from leading edge to roughness element, 12 inches.

Figure 3. - Continued. Recovery-factor distributions at various free-stream Reynolds numbers.

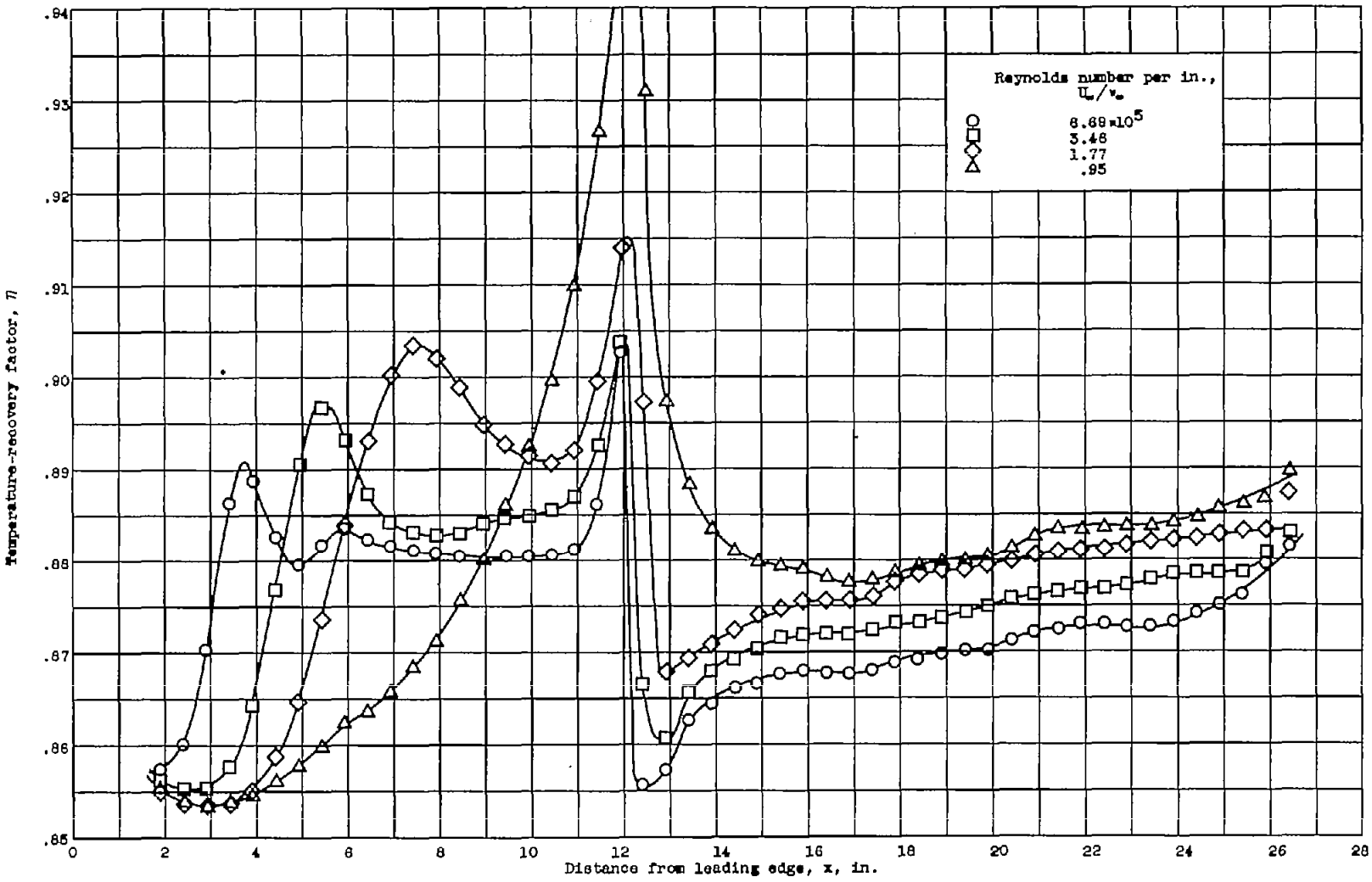

(d) Height of roughness element, 0.079 inch; distance from leading edge to roughness element, 12 inches.

Figure 3. - Continued. Recovery-factor distributions at various free-stream Reynolds numbers.

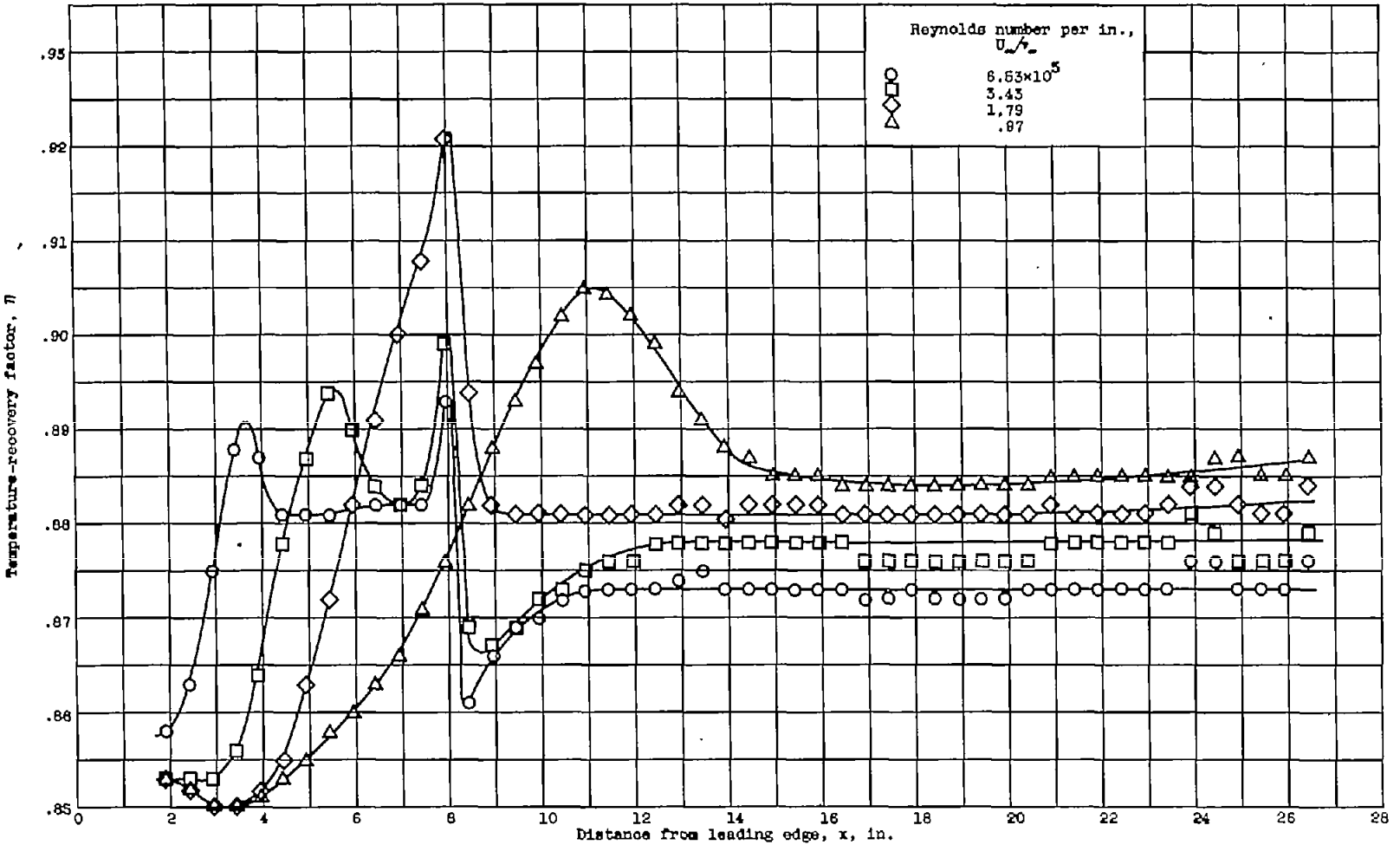

(e) Height of roughness element, 0.032 inch; distance from leading edge to roughness element, 8 inches.

Figure 3. - Continued. Recovery-factor distributions at various free-stream Reynolds numbers.

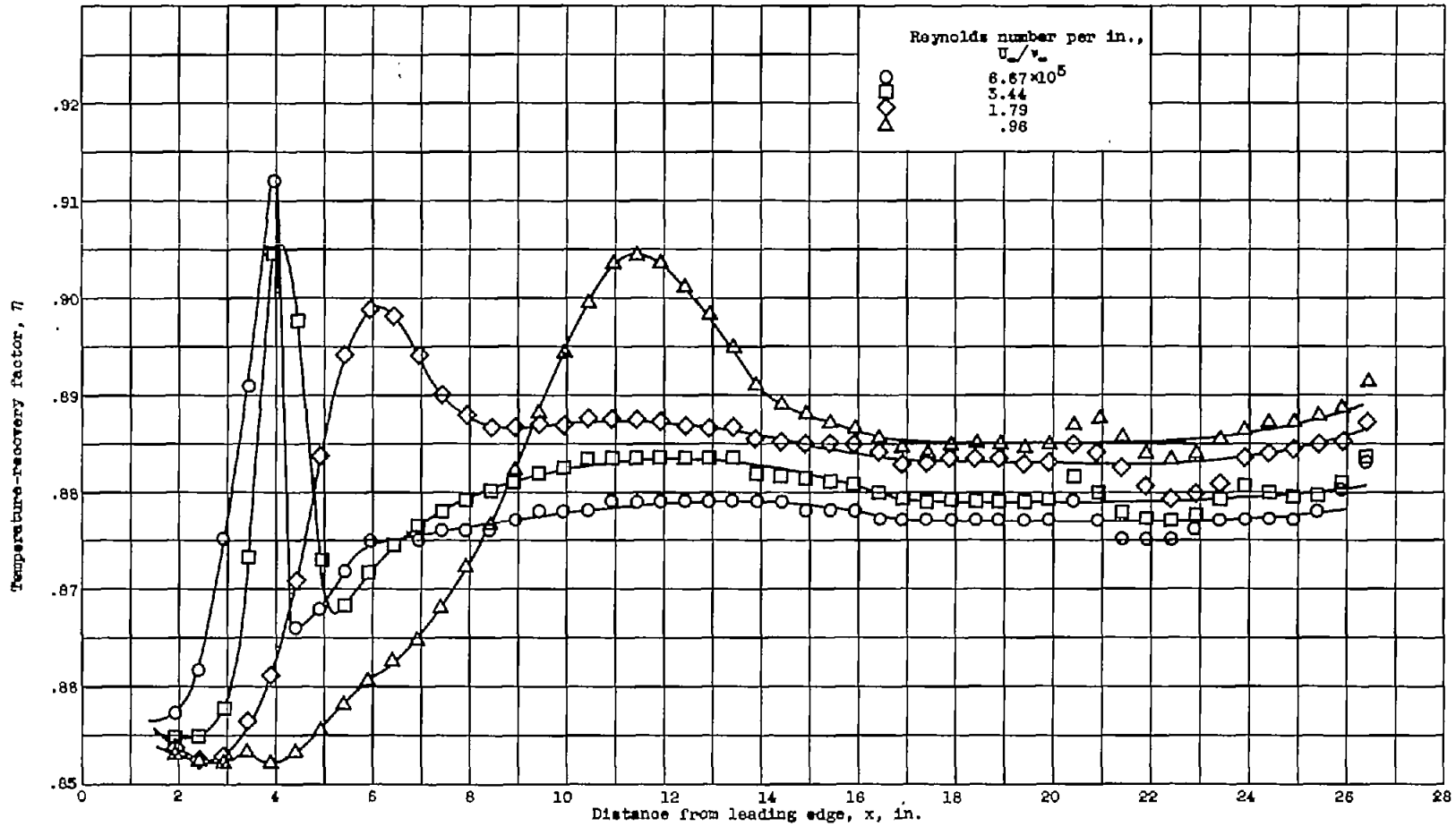

(f) Height of roughness element, 0.032 inch; distance from leading edge to roughness element, 4 inches.

Figure 3. - Continued. Recovery-factor distributions at various free-stream Reynolds numbers.

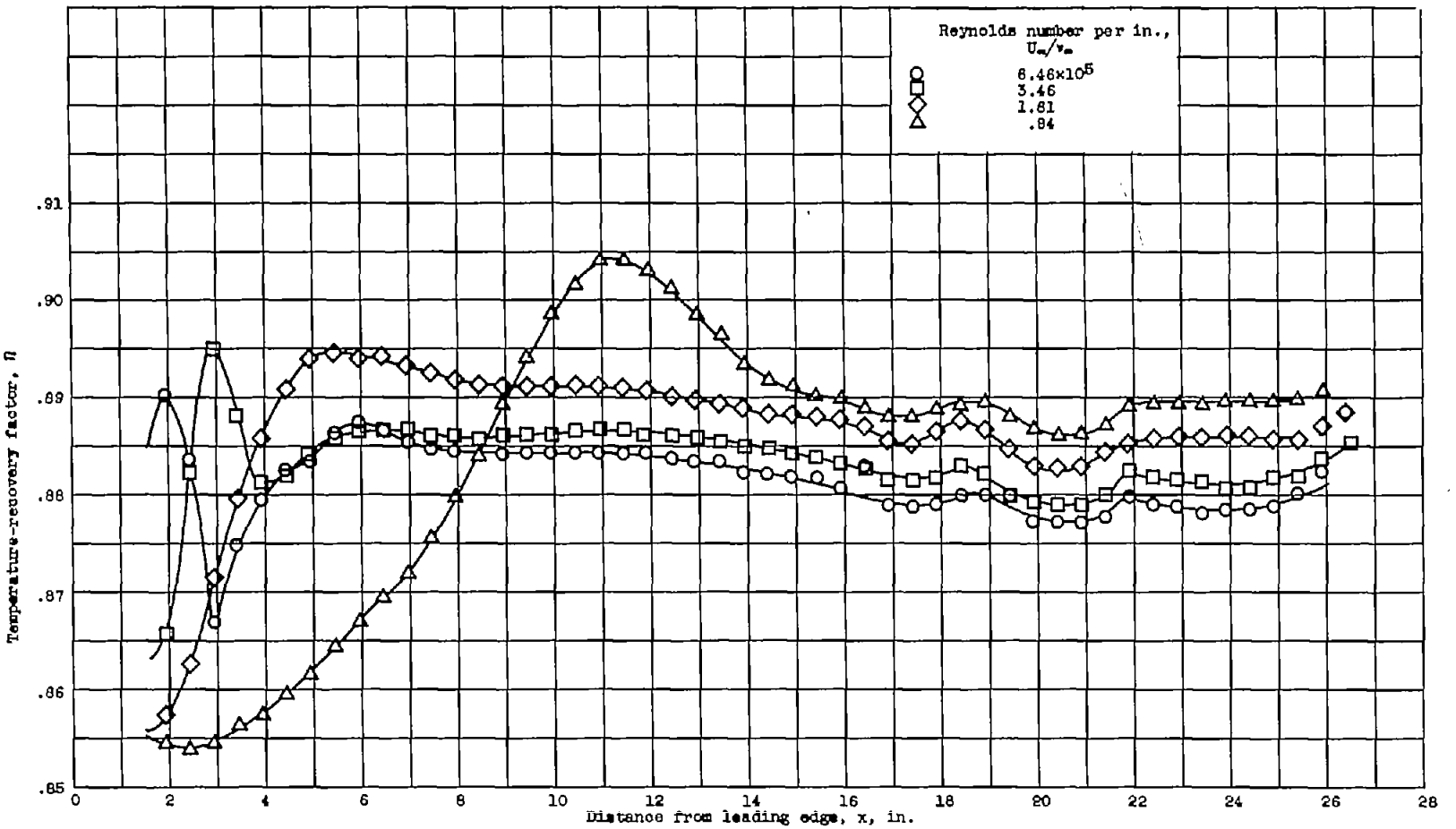

(g) Height of roughness element, 0.032 inch; distance from leading edge to roughness element, 2 inches.

Figure 3. - Concluded. Recovery-factor distributions at various free-stream Reynolds numbers.

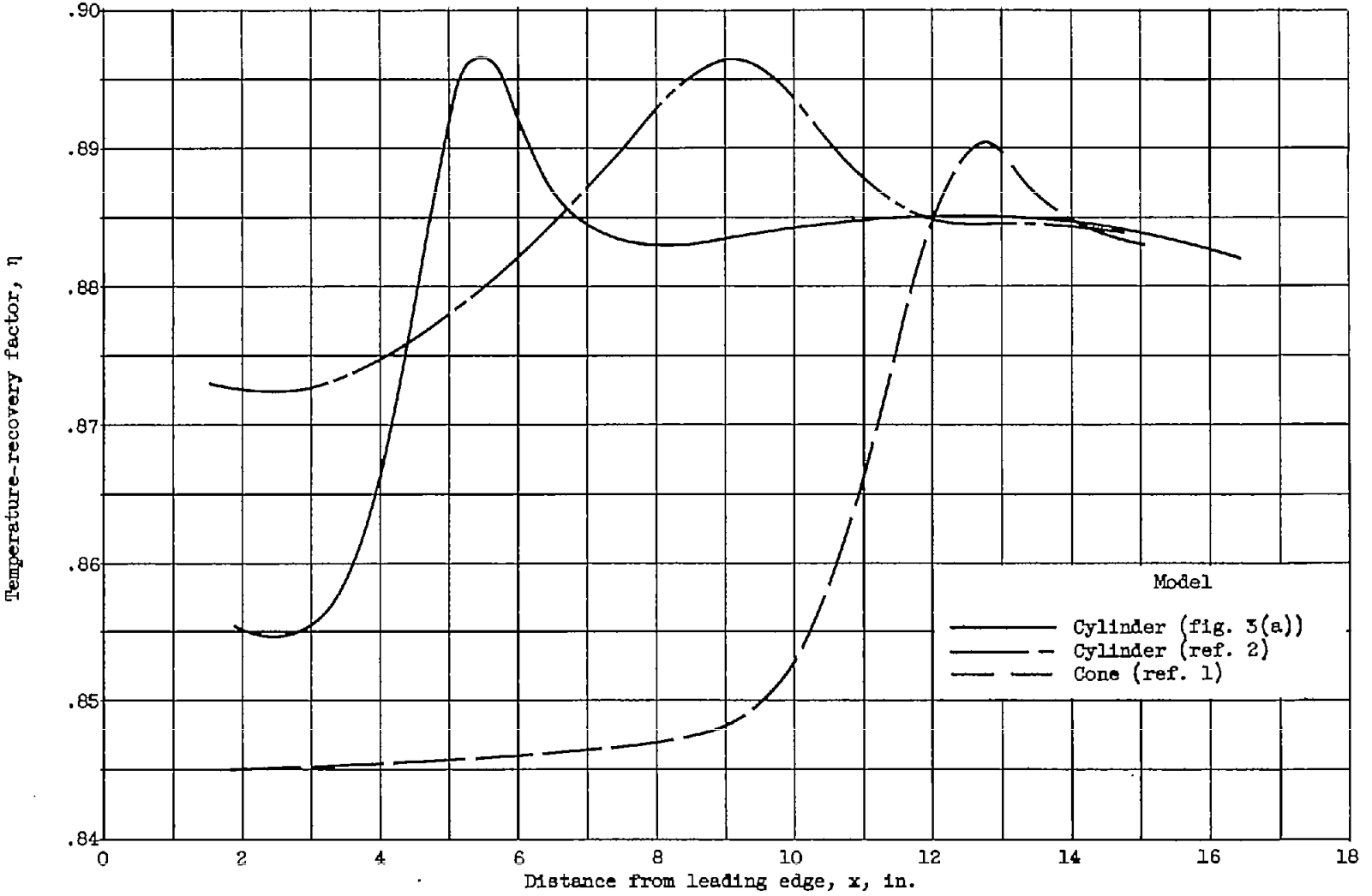

(a) Free-stream Reynolds number, 3.5×10^5 per inch.

Figure 4. - Comparison of recovery factors obtained on various models with no roughness element.

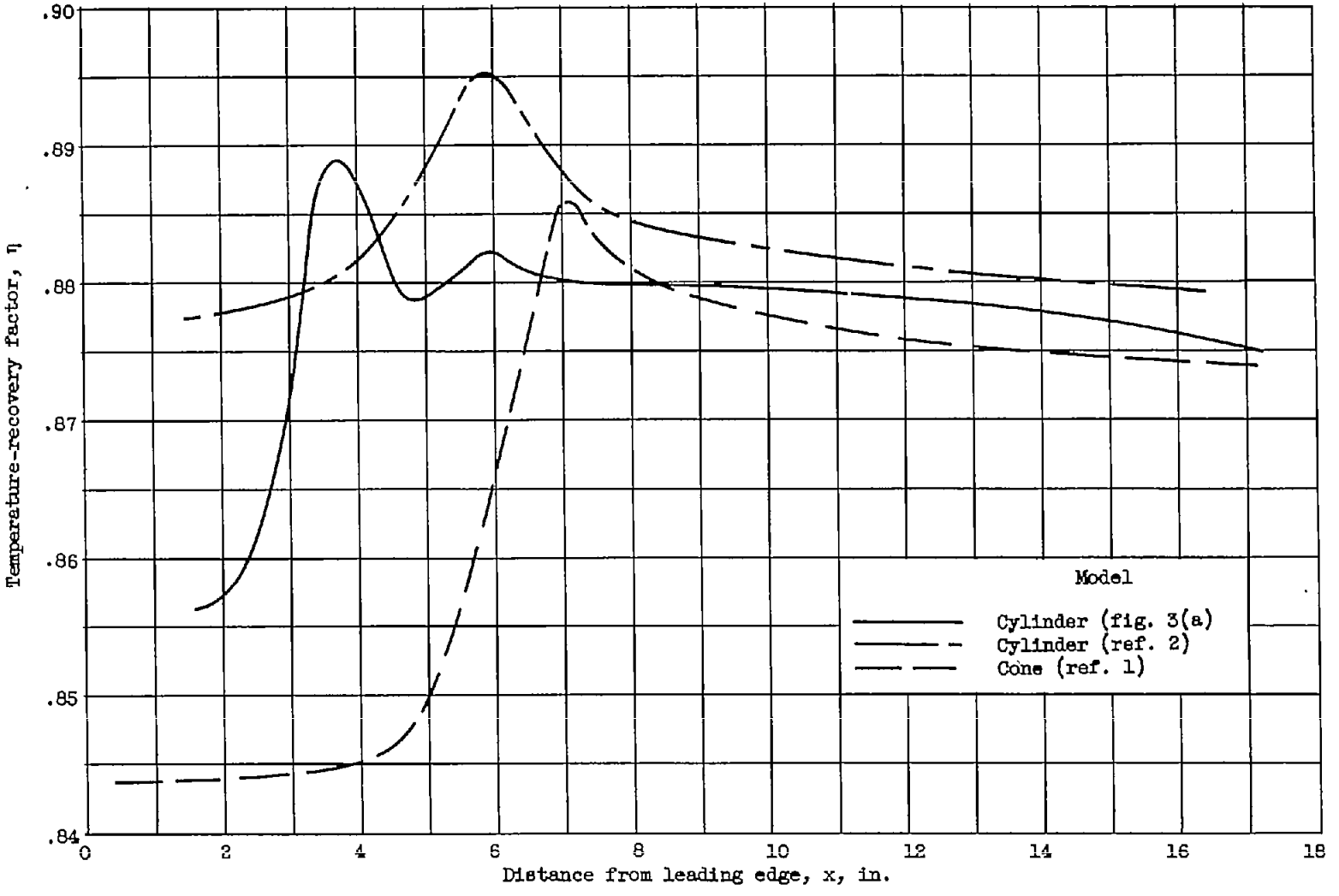

(b) Free-stream Reynolds number, 6.7×10^5 per inch.

Figure 4. - Concluded. Comparison of recovery factors obtained on various models with no roughness element.

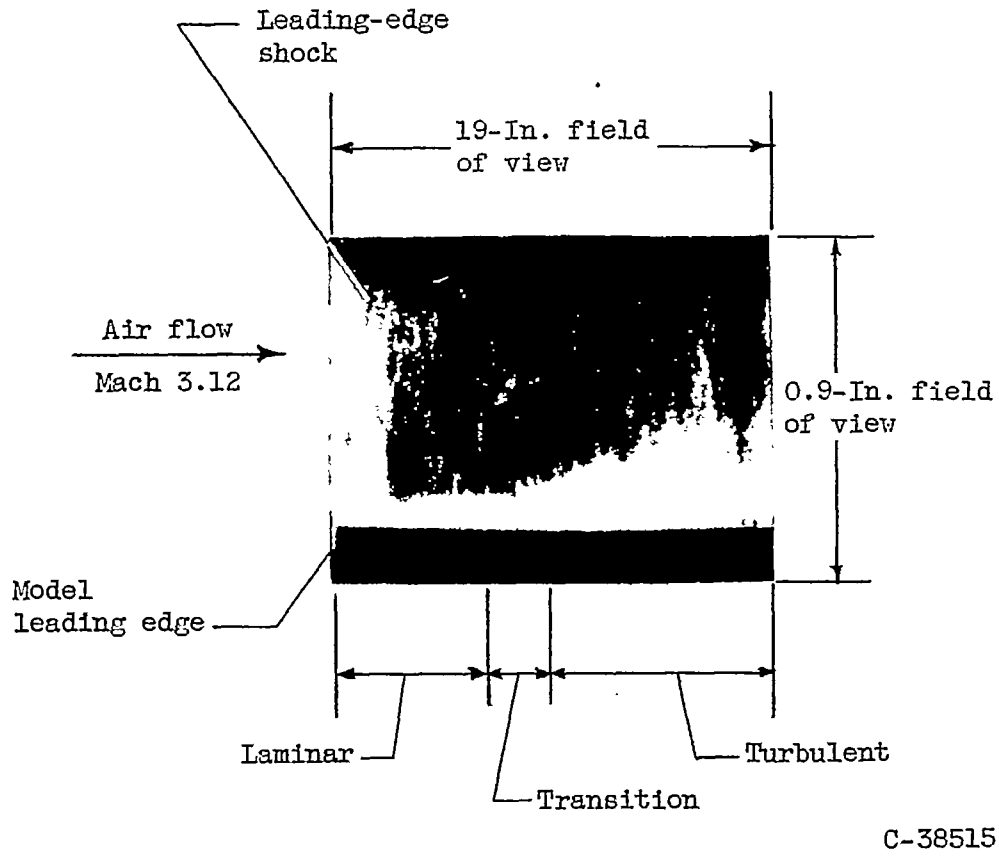

Figure 5. - Enlargement of single high-speed 16-millimeter movie frame showing boundary-layer development. Free-stream Reynolds number, 1.82×10^5 per inch.

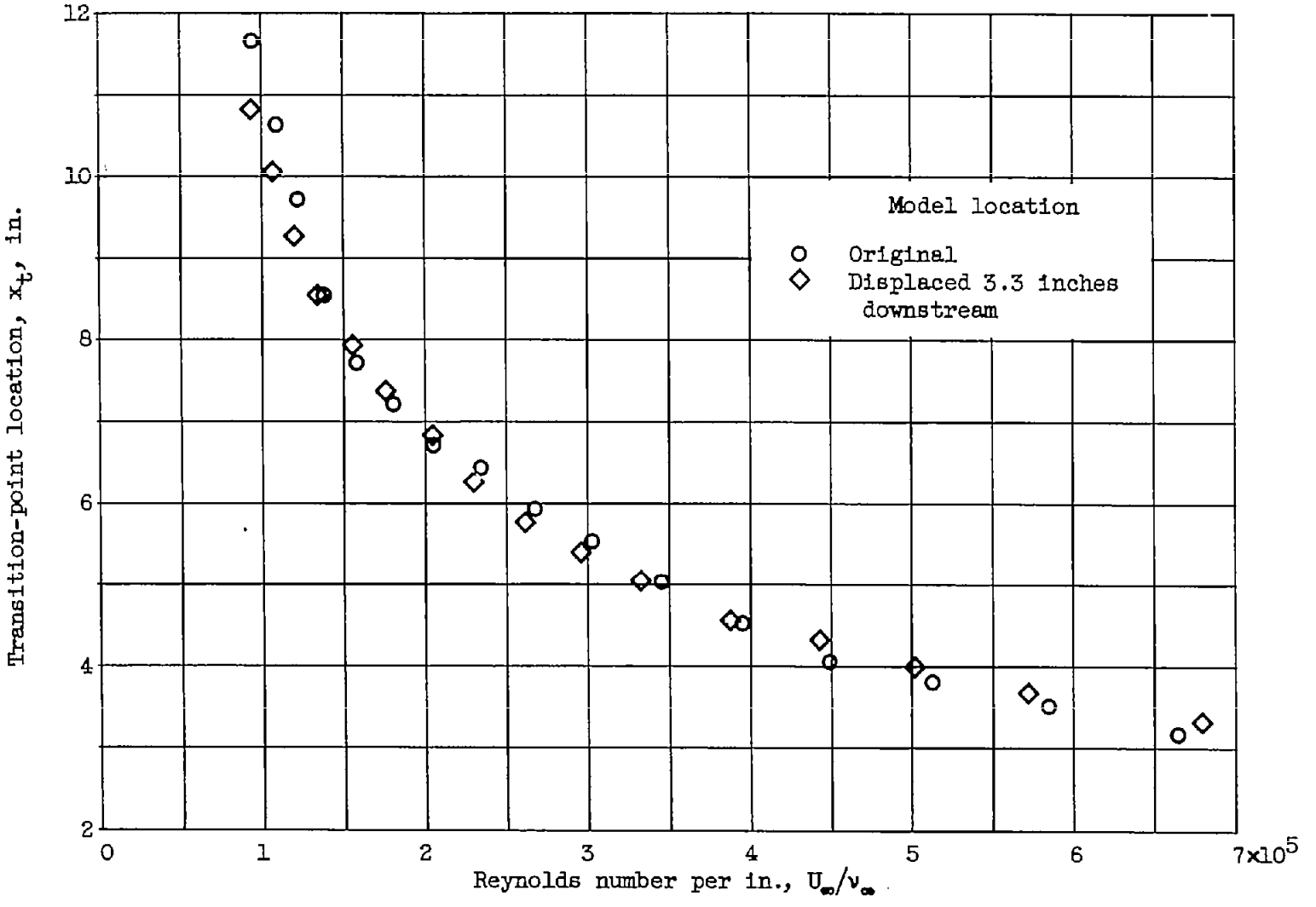

Figure 6. - Effect of free-stream Reynolds number on location of transition point.

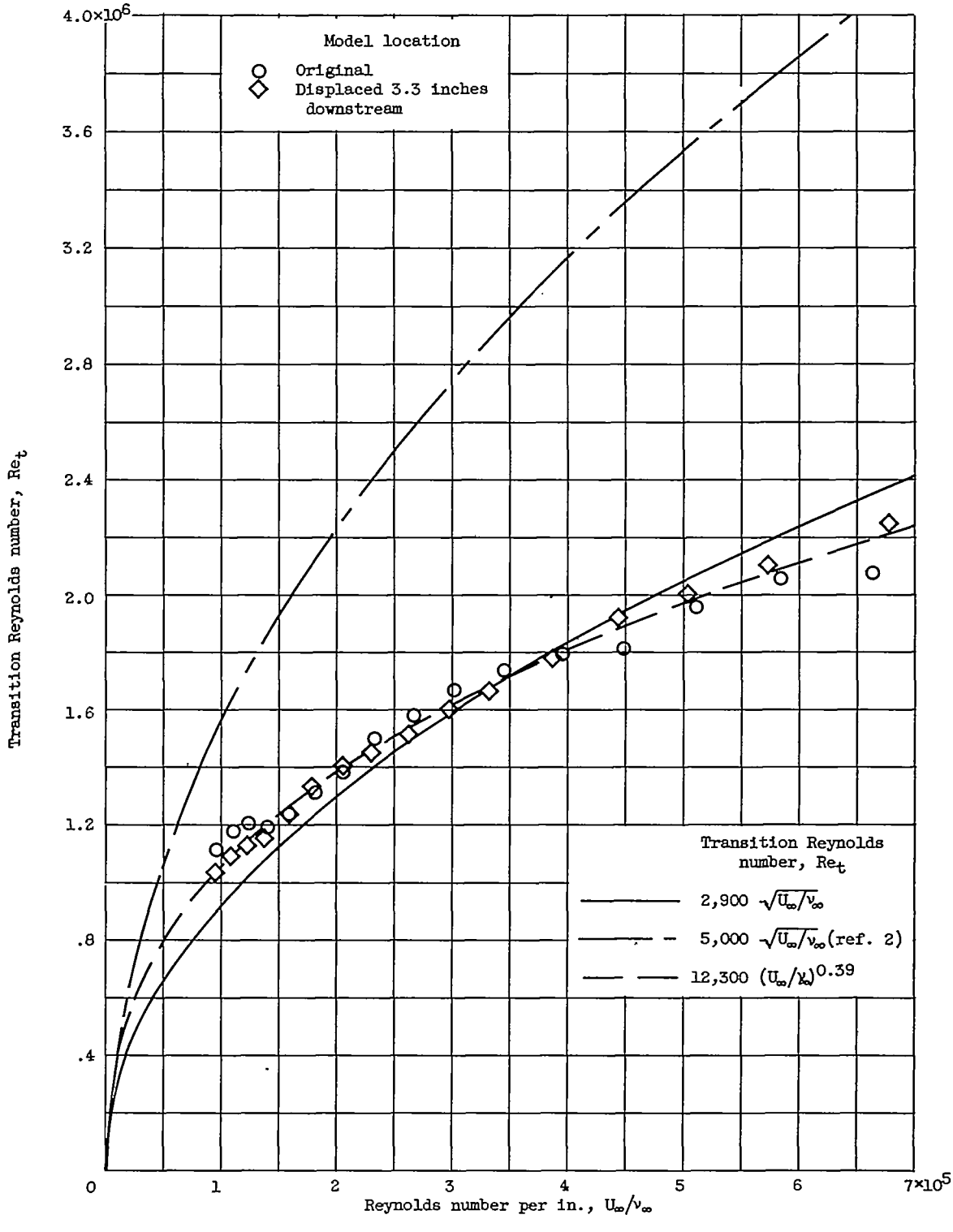

Figure 7. - Effect of free-stream Reynolds number on transition Reynolds number.

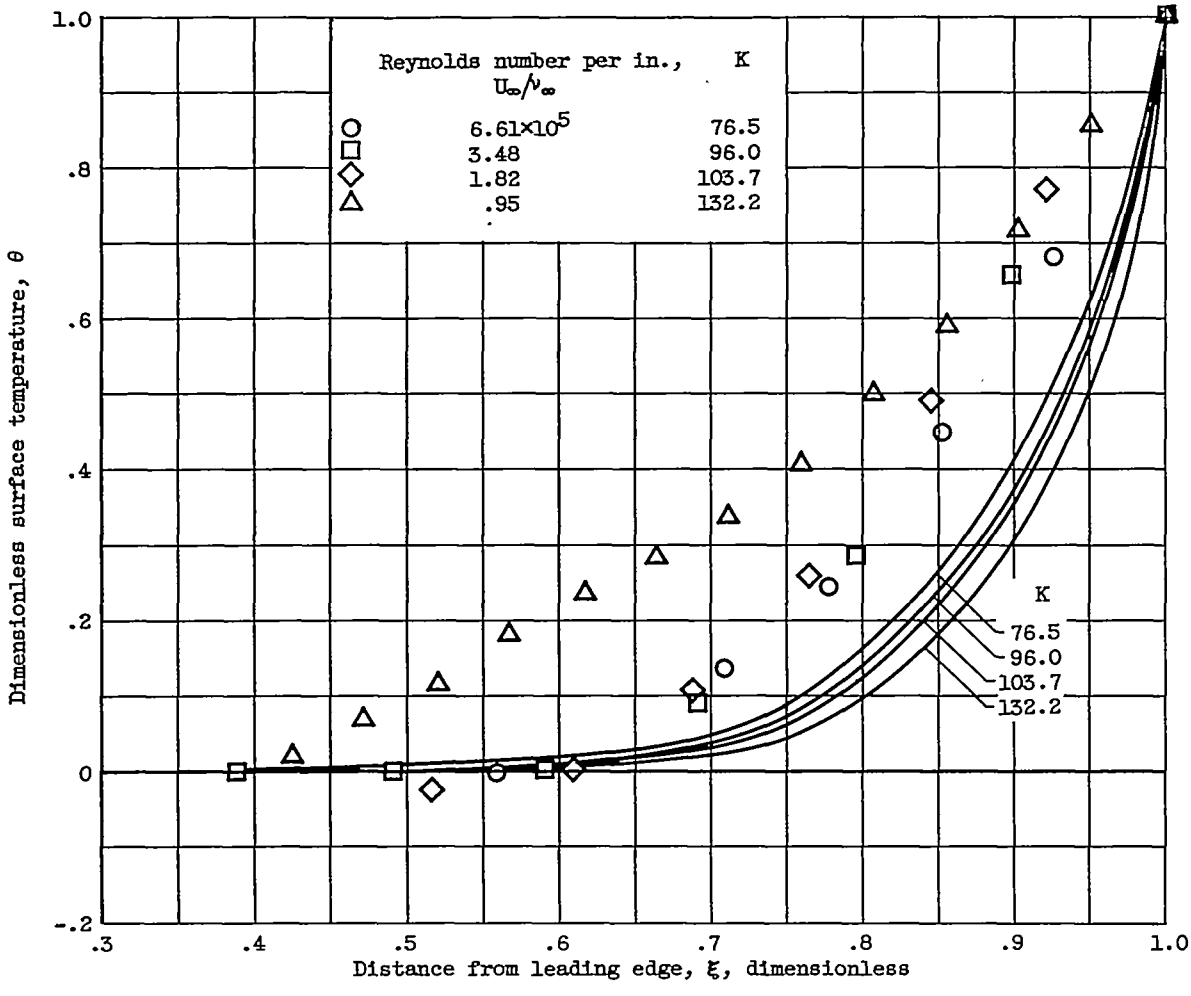

Figure 8. - Effect of surface conduction on temperature distributions.

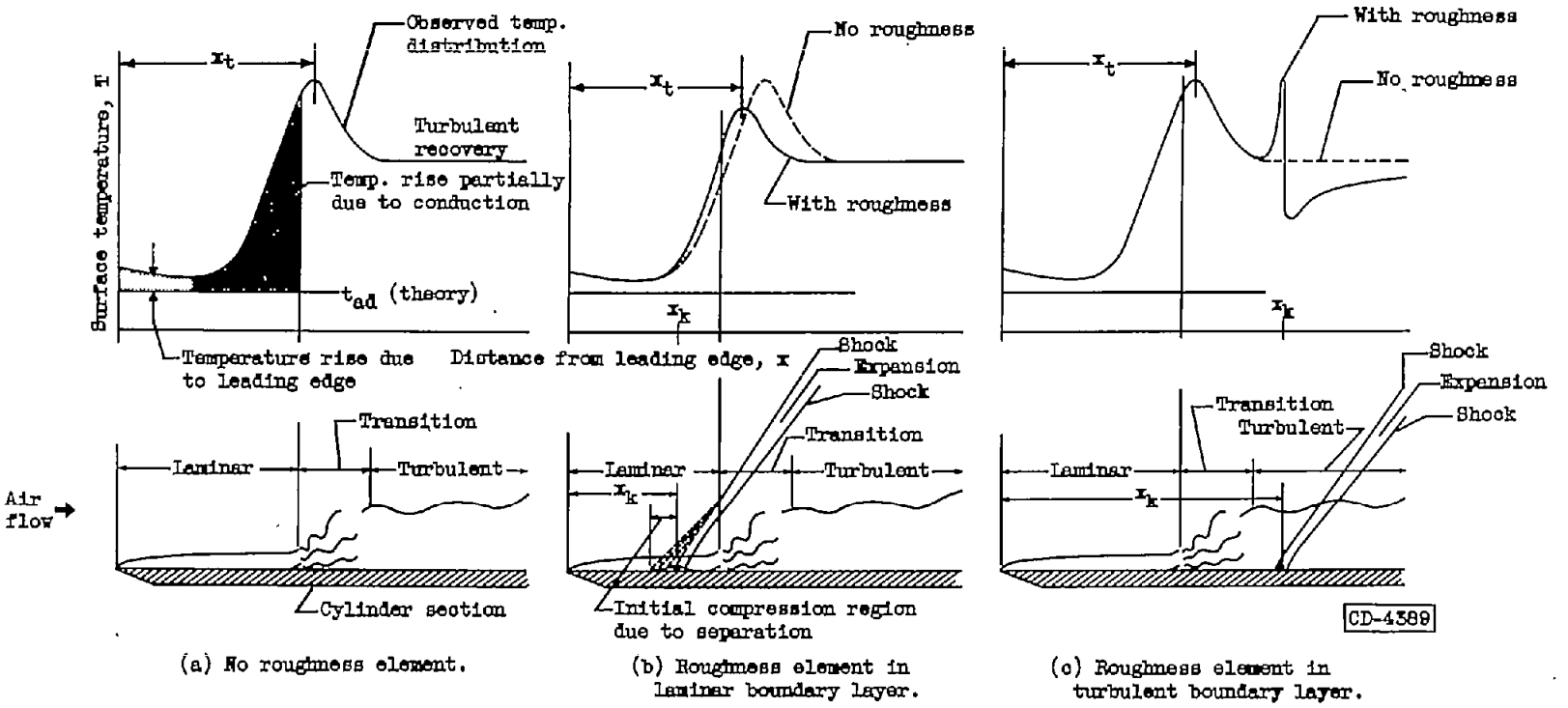

(a) No roughness element.

(b) Roughness element in laminar boundary layer.

(c) Roughness element in turbulent boundary layer.

Figure 9. - Correlation of schlieren observations and temperature distributions.